



1918

TALLINNA TEHNIKAÜLIKOO

TALLINN UNIVERSITY OF TECHNOLOGY

**CHARACTERIZATION AND MODELLING OF
EROSION WEAR OF POWDER COMPOSITE
MATERIALS AND COATINGS**

RENNO VEINTHAL

Faculty of Mechanical Engineering
Department of Materials Engineering
TALLINN UNIVERSITY OF TECHNOLOGY

Dissertation was accepted for the commencement of Degree of Doctor of Philosophy in Engineering on September 29, 2005

Supervisor: Prof., D Sc Eng Priit Kulu, Faculty of Mechanical Engineering

Opponents: Prof., D Sc (Tech) Simo-Pekka Hannula, Helsinki University of Technology, Finland
Sen. Res., D Eng Jüri Pirso, Tallinn University of Technology, Estonia

Commencement: November 11, 2005

Declaration: Hereby I declare that this doctoral thesis, my original investigation and achievement, submitted for the doctoral degree at Tallinn University of Technology has not been submitted for any other degree or examination

Copyright Renno Veinthal, 2005
ISSN 1406-4758
ISBN 9985-59-571-8

INTRODUCTION

Wear in its various modes causes heavy economic losses in industrialized countries. Erosive wear is one of the most common origins of failure in many industrial applications, especially in the mining, oil refinery and pulp and paper industry. In many cases, right materials selection could allow for substantial saving.

To strengthen surfaces of traditional materials (steels), various methods, such as hardening, thermal-chemical treatment and hard coatings are used. Metal-matrix (MMC) materials produced by powder metallurgy have provided a number of new solutions for demanding erosion wear applications. Most of the information available on the tribological properties of these materials has been derived from laboratory tests rather than engineering applications.

Throughout the history, a number of different models and equations have been proposed to predict the erosion of metals and cermets. These models have proven to be incapable of predicting the erosion wear behaviour of MMC materials and coatings, as these contain phases with different hardness-toughness properties.

This study focuses on the relations between the properties of MMC materials and coatings and their wear behaviour. In addition, an attempt is made to characterize the response of selected materials to erosion and high-energy impact. This new knowledge contributes to the development of new wear resistant materials for specific wear environments.

Acknowledgements

I would like to express my special thanks to my supervisor Prof. Priit Kulu, Head of the Department of Materials Engineering of TUT, for his support, guidance and encouragement, which made this work possible.

My special gratitude belongs to Prof. Helmo Käerdi from the The Department of Mathematics, Estonian National Public Service Academy, for continuous discussions and advice concerning mathematical processing of the experimental data.

I would like to thank Sergei Zimakov and Irina Hussainova for their contributions to the publications. My thanks are due to all my colleagues from the Department of Materials Engineering of TUT for their assistance and support, especially to Ahto Vallikivi, Peeter de Bakker, Georg Våljaots, and Riho Tarbe for materials preparation, analysis and wear testing, to Valdek Mikli from Materials Research Centre for materials characterization and to MSc. student Allan Aulik for material testing and specimen preparation.

During my PhD studies I had the pleasure of collaborating with material scientists from Tampere University of Technology and Uppsala University. My special thanks go to Prof. Petri Vuoristo and Prof. Sture Hogmark for that splendid opportunity.

Fruitful cooperation with Jari Liimatainen and Pekka Siitonen from Metso Powdermet OY provided experimental data on the wear behaviour of composite materials and coatings. Their efforts are highly appreciated.

Estonian Science Foundation (grant no. 5881) is acknowledged for supporting my research. The Centre for International Mobility CIMO, Archimedes Foundation and Estonian Academic Foundation for International Exchange are acknowledged for covering my travel and living costs abroad.

Finally, I would like to thank my family and friends for their help and encouragement.

CONTENT

LIST OF PUBLICATIONS.....	5
1 REVIEW OF THE LITERATURE.....	7
1.1 Materials for wear applications.....	7
1.2 Erosion wear resistance of powder materials and coatings.....	7
1.2.1 Erosion of hardmetals.....	7
1.2.2 Erosion of ceramics.....	8
1.2.3 Erosion of coatings.....	9
1.3 Modelling of erosive wear.....	10
1.4 Indentation as a method for characterizing the hardness-toughness properties of materials.....	11
1.4.1 Methods of indentation.....	11
1.4.2 Hardness characterization.....	12
1.4.3 Characterization of fracture toughness.....	14
1.5 Objectives of the study.....	15
2 MATERIALS AND EXPERIMENTAL.....	17
2.1 Studied materials.....	17
2.2 Indentation method for the characterization of materials.....	18
2.2.1 Hardness measurements.....	18
2.2.2 Determination of fracture toughness and fracture probability.....	19
2.3 Erosion testing.....	20
2.3.1 Erosion tester.....	20
2.3.2 Used erodents.....	21
2.3.3 Study of worn surfaces.....	23
3 CHARACTERIZATION OF POWDER COMPOSITE MATERIALS AND COATINGS USING INDENTATION.....	24
3.1 Hardness characterization of the MMC material with multimodal reinforcements.....	24
3.2 Hardness characterization of MMC coating.....	27
3.3 Fracture toughness and fracture probability of the hard phase.....	27
4.1 Erosion resistance of MMC materials.....	29
4.2 Erosion resistance of MMC coatings.....	31
4.3 Wear mechanisms.....	32
5 CALCULATION OF EROSION WEAR USING PARAMETERS DETERMINED BY DIFFERENT INDENTATION METHODS.....	37
5.1 Calculation principles.....	37
5.2 Calculation of erosion rate of MMC material.....	38
5.3 Calculation of erosion rate of MMC coating.....	41
CONCLUSIONS.....	44
References.....	47
KOKKUVÖTE.....	49
Paper I.....	56
Paper II.....	57
Paper III.....	58
Paper IV.....	59
Paper V.....	60
Paper VI.....	61

LIST OF PUBLICATIONS

The present dissertation is based on the following papers, which are referred in the text by their Roman numerals I–VI. As some of the recent research have not been published yet, this thesis was somewhat enlarged.

I. Kulu, P., Veinthal, R.

Selection criteria for abrasive erosion wear resistant powder coatings, *Materials Science (Medžiagotyra)*, Vol. 8, No 4, 2002, pp. 409–412.

II. Veinthal, R., Kulu, P., Käerdi, H.

Characterization of the structure of composite powder materials and coatings, *Materials Science (Medžiagotyra)*, Vol. 11, No. 4, 2005, pp. 376–380.

III. Kulu, P., Veinthal, R., Käerdi, H.

Modelling of erosion wear of powder composite materials and coatings, *International Journal of Tribology* (submitted)

IV. Kulu, P., Hussainova, I. and Veinthal, R.

Solid particle erosion of thermal sprayed coatings, *Wear*, Vol. 258, 1–4, 2005, p. 488–496.

V. Kulu, P., Veinthal, R.

Wear resistance of high velocity thermal sprayed coatings, *Proc. of 9th Nordic Symposium on Tribology NORDTRIB 2000*, VTT of Finland, Espoo, Finland, 2000, Vol. 1, pp. 87–95.

VI. Kulu, P., Veinthal, R., Kõo, J., Lille, H.

Mechanism of abrasion erosion wear of thermal sprayed coatings, *Proc. of the Conference EUROMAT 2000 on Advances in Mechanical Behaviour, Plasticity and Damage*, Tours, France, 2000, pp. 651–656.

Other publications (not included in the thesis)

VII. Kulu, P., Veinthal, R.

Characterization of the structure and modelling of wear of composite powder materials and coatings with multimodal reinforcement, *XII Annual International Conference on Composites/Nano Engineering ICCE-12*, Tenerife, 2005, CD-ROM.

VIII. Veinthal, R., Kulu, P., Aulik, A., Siitonen, P.

Environmentally assisted abrasive-erosive wear of metal matrix composites, *Materials Technology Innovations, Conference on Powder Metallurgy and Advanced Materials*, Tampere, 2005.

IX. Veinthal, R., Zimakov, S., Kulu, P.

Micromechanical properties and wear resistance of powder coatings, *Proc. of the 3rd International DAAM Conference*, Tallinn, Estonia, 2002, pp. 216–219.

X. Zimakov, S., Tarbe, R., Veinthal R., Kulu, P.

Optimization of structure of sprayed WC-Co hardmetal based coatings, *Proc. of the 3rd International DAAM Conference*, Tallinn, Estonia, 2002, pp. 224–229.

XI. Kulu, P., Ojaviir, M., Veinthal, R.

Study of properties of HVOF- sprayed coatings, *Proc. of the 2nd International DAAAM Conference*, Tallinn, Estonia, 2002, pp. 214–217.

Approbation

International conferences

1. 10th Nordic Symposium on Tribology NORDTRIB 2002, 9–12 June 2002, Stockholm, Sweden
2. European Congress on Advanced Materials and Processes EUROMAT 2005, 5–8. September 2005, Prague, Czech Republic
3. 14th International Baltic Conference MATERIALS ENGINEERING 2005, 6–7 October 2005, Kaunas, Lithuania

1 REVIEW OF THE LITERATURE

1.1 Materials for wear applications

To strengthen surfaces of traditional materials (steels), various methods, such as hardening, thermal-chemical treatment and hard coating are used. They are meant to reduce the operation wear of parts and processing tools in the conditions of abrasive wear.

High surface hardness of traditional materials does not always provide the wear resistance required for faultless operation of tools under the conditions of wear caused by contact pressure, high speed and fatigue processes. Thus, toughness parameters of materials are as important as their hardness parameters (Fig 1.1).

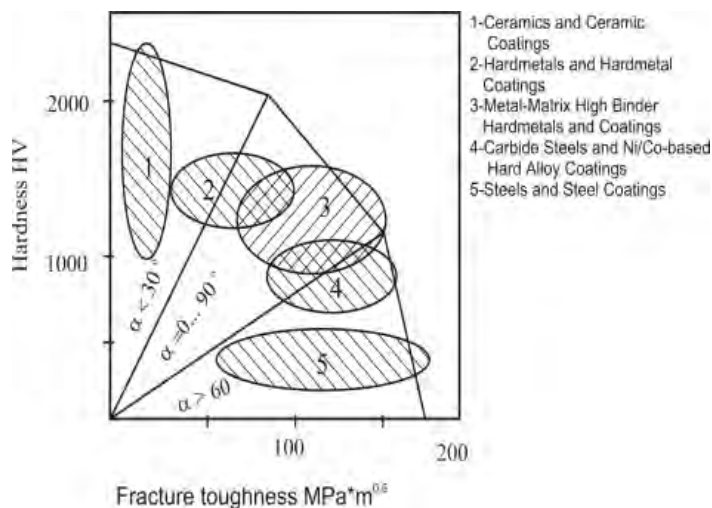


Figure 1.1 Hardness-toughness properties of different material groups

Tribological materials and coatings are typical of heterogeneous structure: hard particles in a relatively soft metal matrix. Under the abrasive wear conditions, tungsten carbide based or containing systems are most widely used and highly effective. Due to the high hardness of tungsten carbide and toughness of the binder metal or metal matrix – this group of materials and coatings has a good combination of “hardness-toughness” properties. They are widely used for erosion protection of machine parts and tools. Along with the methods of traditional materials and metals processing, such as heat treatment, thermochemical treatment and coating, to obtain the complex of the “hardness-toughness” properties, powder technology is the most promising. The main advantage of this technology is the possibility of producing materials surfaces with special composition and properties, i.e. wear resistant materials and coatings.

Examples of that kind of materials with multimodal reinforcement are the so-called “double-cemented” materials and coatings. These metal-matrix composites contain two kinds of reinforcement – coarse carbides of some hundreds μm and micrometrical or sub-micrometrical carbide particles divided evenly in the matrix phase.

1.2 Erosion wear resistance of powder materials and coatings

1.2.1 Erosion of hardmetals

Wear resistance of traditional tungsten carbide-cobalt (WC-Co) based hardmetals has been studied in different conditions of abrasive wear because of their wide range of applications. Erosive wear related

studies have been conducted on WC-Co as the most common hardmetal. A systematic study of erosion resistance of different hardmetals and cermets using silicon oxide particles as an abrasive was conducted by researchers of TUT [2-5].

Tungsten carbide-cobalt based hardmetals with cobalt content from 6 to 30 % were studied. Their hardness HV10 varied from 890 to 1429 at Co content 30% and 6%, respectively. The volumetric wear rate and relative erosion resistance of hardmetals are given in Table 1.1.

Table 1.1. Erosion resistance of WC-Co based hardmetals (abrasive – quartz sand 0.1 - 0.3 mm, $v = 80$ m/s, $\alpha = 30^\circ$, reference material steel 0.45% C, 210 HV)

Composition, wt%	Erosion rate, mm ³ /kg	Relative erosion resistance ε
WC-6Co	0.32	75.3
WC-8Co	0.45	53.3
WC-10Co	1.90	12.7
WC-15Co	3.30	7.3
Steel 0.45% C	24.1	1.0

1.2.2 Erosion of ceramics

Erosion characteristics at abrasive wear of different types have been studied by numerous researchers. One of the first studies of experimental engineering ceramics on hard particle erosion was conducted on a centrifugal type tester with quartz sand [6]. Tests covered the range of particle velocities from 26 to 80 m/s, the impact angles ranging between 15 and 90°. It was established that unlike steels, generally, ceramics is only slightly influenced by changes in the impact velocity, hence, their relative wear resistance increases at higher impact velocities. Resistance will also increase with the decrease of the impact angle (Fig 1.2).

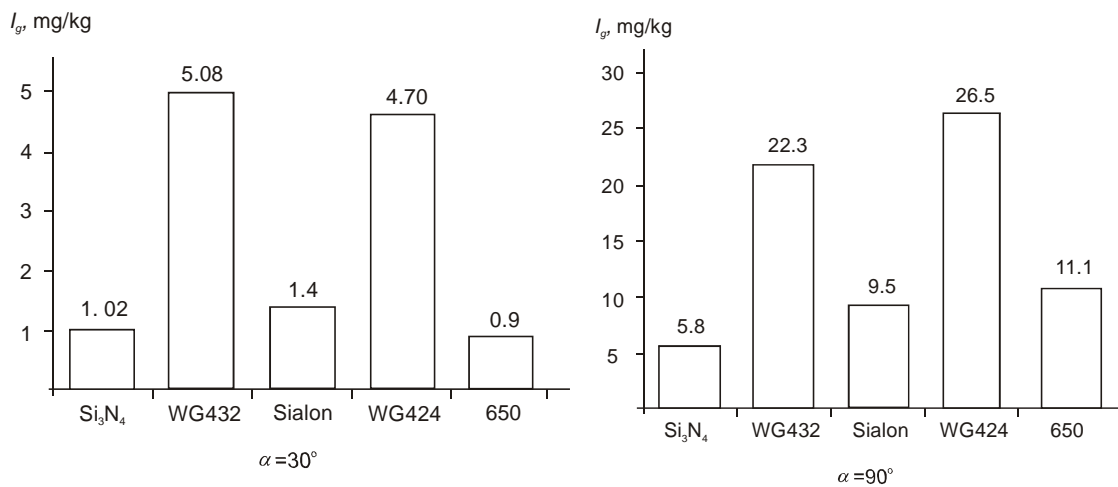


Figure 1.2 Erosion rate of ceramics

According to the results obtained, the four types of ceramics under study were arranged in the following order: Si₃N₄ (most resistant), SiC, ZrO₂, and Al₂O₃ (Table 1.2).

Table 1.2. Erosion resistance of different ceramics (abrasive – quartz sand 0.1 - 0.3 mm, $v = 76$ m/s, reference material steel 0.45% C, 210 HV)

Target material (wt%) and hardness	Density ρ , kg/m ³	Relative erosion resistance ε		
		$\alpha=15$	$\alpha=45$	$\alpha=90$
Al ₂ O ₃ , 1320 HV	3700	4.4	12.0	0.5
ZrO ₂ , 1110 HV	5700	6.6	0.9	0.2
SiC, 2710 HV	3100	11.8	11.7	3.1
Si ₃ N ₄ -5 Al ₂ O ₃ -8Y ₂ O ₃ , 1750 HV	3300	41.2	101	43.4

Erosion resistance of different commercially available engineering ceramics at hard-particle erosion with different erodents was investigated at TUT. Studies covered the following types of ceramics: alumina, silicon nitride and Sialon (Table 1.3).

Table 1.3. The ceramics studied [6]

Grade	Composition	Hardness HV	Fracture toughness K_{Ic} , $N/mm^2 \cdot m^{0.5}$
WG 432	Al_2O_3	1800	4.0
650	$Al_2O_3 + TiC$	3600	4.0
690	$Si_3N_4 + ZrO_2$	2500	6.0
WS 09597 (Sialon)	SiAlON	2600	7.7

Erosion tests of ceramics by erosion at 61 m/s with SiO_2 (at 30 and 45°) showed that higher erosion resistance was demonstrated by Al_2O_3 and Sialon. At normal impact, ceramics is characterized by erosion wear being maximal at the impact angle of 90°.

1.2.3 Erosion of coatings

Kulu [7] was one of the first to study the erosion of thermal sprayed coatings – detonation sprayed hardmetal-type coatings. It was shown that the erosive wear resistance of coatings from powder mixtures (WC and Co) was low; the coating from sintered hardmetal powder has the highest relative wear resistance (Table 1.4).

Table 1.4. Composition, hardness and erosion resistance of hardmetal-type coatings

Composition, wt%	Hardness HV 0.05	Relative erosion resistance ϵ	
		$\alpha=30^\circ$	$\alpha=90^\circ$
WC-9Co (agglomerated and sintered)	1310	3.1	1.1
WC-9Co (mechanical mixture)	1220	1.8	0.2
WC-20Co (mechanical mixture)	810	1.4	0.4

A systematic erosion study of thermal sprayed high-velocity oxy-fuel sprayed (HVOFS) and flame spray fused (FSF) coatings was also conducted by Kulu and others at TUT [8, 9].

The studied hardmetal-type or hardmetal containing coating groups may be classified as

- HVOFS WC-Co-based coatings,
- FSF Ni-based self fluxing alloy coatings,
- FSF composite NiCrSiB-(WC-Co) coatings.

The erosion resistance of the selected coatings is given in Table 1.5.

Table 1.5. Erosion resistance of thermal sprayed coatings [8, 9]

Deposition method	Composition of coating, wt%	Hardness HV 0.2	Relative erosion resistance ϵ	
			$\alpha=30^\circ$	$\alpha=90^\circ$
Detonation spray	WC-9 and 15 Co	1155-945	3.1-2.8	1.1
HVOFS	WC-17Co (Tafa 1343 VM)	1300	11.2	2.6
	NiCr16Si4Fe4B3.5 (Tafa 1275H)	805	0.6	0.4
FSF	NiCrSiB-based coatings	430-700	1.3-1.6	0.8-0.4
	NiCrSiB-(15-50) (WC-15Co)	675-735/ 1410-1465*	1.5-2.0	0.7-0.6

*matrix/hard phase

It follows from the experiments that hardness has a major effect on the wear of materials by the mechanisms of plastic deformation, while fracture toughness is a dominant factor in the wear, involving a brittle fracture. An interesting group of thermal sprayed coatings is based on NiCrSiB-matrix, with WC-Co hardmetal as reinforcement [8, 9]. It was demonstrated that matrix hardness, WC-Co grain size and WC-Co content has an effect on the erosion rate: the wear resistance of coatings increases with an increase in matrix hardness as well with an increase in the hard phase content in the composite at low impact angles of particles.

Thermal sprayed ceramic coatings studied by Kulu [7] showed very low erosion wear resistance – one order lower than that of the reference material – steel 0.45% C (Table 1.6). Low wear resistance of ceramic coatings is caused by their brittleness and relatively high porosity.

Table 1.6 Erosion resistance of thermal sprayed ceramic coatings [7]

Composition, wt%	Hardness HV 0.05	Relative erosion resistance ε	
		$\alpha=30^\circ$	$\alpha=90^\circ$
Al ₂ O ₃ (plasma sprayed)	950	0.1	0.02
TiO ₂ (plasma sprayed)	1100	0.1	0.02
Cr ₃ C ₂ (detonation sprayed)	930	1.6	0.4

1.3 Modelling of erosive wear

A number of empiric relations to calculate the wear volume of bulk homogeneous materials using hardness, Young modulus E and toughness K_{1c} have been proposed [10, 11].

Beckmann, Kleis and Gotzmann developed the models of plastic deformation and brittle fraction for homogenous materials [12,13].

According to Beckmann and Kleis [12], weight wear rate from plastic deformation I_g^p can be expressed as follows:

$$I_g^p = \frac{3}{4\pi} \cdot \frac{\rho_1}{\rho_2} \cdot \frac{\tau_0}{e_s} \left[6.81 \left(\frac{h_p}{R_2} \right)^{0.5} \cdot \frac{2\rho_2}{3H_1} v_0^2 \cdot \cos^2 \alpha + 0.85 \left(\frac{h_p}{R_2} \right)^2 \right]. \quad (1.1)$$

Eq. (1.1) is valid if the hardness of abrasive particles H_2 has to exceed that of material H_1 by 1.6 times as a minimum. According to Gotzmann [13], weight wear rate from brittle fracture

$$I_g^b = \frac{\Delta m}{M} = \frac{\pi \cdot C_r^2 h_l \cdot \rho_1}{\left(\frac{4}{3}\right)\pi R_2^3 \rho_2} = 0.75 \cdot \sqrt{3} \frac{\rho_1}{\rho_2} \left(\frac{C_r}{R_2} \right)^2 \cdot \left(\frac{h_p}{R_2} \right)^{0.5}, \quad (1.2)$$

where ρ_1 and ρ_2 – density of the material and abrasive particle, R_2 – radius of the abrasive particle, H_1 – hardness of the material, v_0 – particle velocity, α – impact angle, h_p – depth of penetration/indentation, C_r – length of the radial crack, h_l – depth of the lateral crack, τ_0/e_s – shear energy density.

According to Beckmann and Kleis [12], the ratio τ_0/e_s is a universal parameter used to determine the wear resistance of metals at plastic deformation. On the basis of statistical data, a graph (Fig. 1.3) has been composed on pure metals, carbon and alloy steels and white cast irons [12]. According to Gotzmann, crack initiation and propagation are the main processes occurring at brittle fracture.

According to the models of erosion wear developed and verified by Beckmann and Gotzmann, the following parameters characterizing materials were found necessary:

- shear energy density τ_0/e_s , characterizing material removal at plastic deformation;
- parameters of hardness distribution;
- fracture toughness, characterizing the brittle fracture mechanism;
- fracture probability parameter,

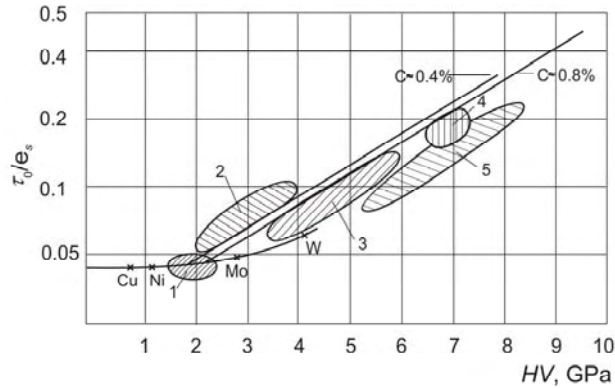


Figure 1.3 Variation of τ_0/e_s as a function of initial hardness HV of the target material: 1 – austenitic manganese steels, 2 – non-alloy and low-alloy steels, 3 – alloyed (with Mn, Si, Cr) and cast steels, 4 – hardened steels, 5 – high carbon and high-alloy steels (high speed, ledeburitic etc), white cast irons

Heterogeneous materials, such as MMC materials require that two different erosion theories (plastic deformation and brittle fracture) be taken into consideration. A relatively soft metal matrix requires a model of plastic deformation and the hard phase needs both of the models: the plastic deformation and brittle fracture models of wear, involving the material parameters such as hardness and toughness.

The wear behaviour of composite materials that have a relatively soft metal matrix, containing about 20–50 vol% evenly distributed hard phase of high hardness can hardly be calculated using empiric equations of Beckmann and Gotzmann. The behaviour of different phases must be taken into account in the calculation of wear.

The contact radii, as they appear with the wear caused by solid particle erosion, lie in general in the scale of grain dimensions. Therefore, hardness distribution must be considered. It is evident that the increase in the kinetic energy of an abrasive particle leads to the increase in the indentation depth. The effective force as well as the portion of brittle fracture grows in the impact area. The rise of the kinetic energy can be reached either by the increase of the speed or the mass of the abrading particle.

The question arises – how to characterize this type of structures and to determine the hardness-toughness properties?

1.4 Indentation as a method for characterizing the hardness-toughness properties of materials

1.4.1 Methods of indentation

The method of continuous indentation or the depth sensing hardness test concerns the measurement of force and displacement during the penetration of the indenter (diamond pyramid) into the material. As the method avoids a direct human influence on the measurement process, the method is also called instrumented hardness or universal hardness HU . Proposed by Weiler [14], it is based on the use of Vickers pyramid and will be calculated as the quotient of indentation force by the contact area between the indenter and the specimen.

$$HU = \frac{F}{26.43(h - h_0)^2}, \quad (1.3)$$

where $(h - h_0)$ – actual penetration depth into the specimen.

The denominator in Eq (1.3) is the contact area between the indenter and the specimen. The indenter is considered as an ideal Vickers pyramid with its tip angle of 136° between opposite facets. The determination of the exact contact point between the indenter tip and the material surface can be difficult. If the material is homogeneous and the tip geometry is ideal, the universal hardness can be calculated from the slope of the plot of square-root force against displacement (Fig 1.4).

$$HU_s = 0.0378 \cdot \left(\frac{d\sqrt{F}}{dh} \right)^2. \quad (1.4)$$

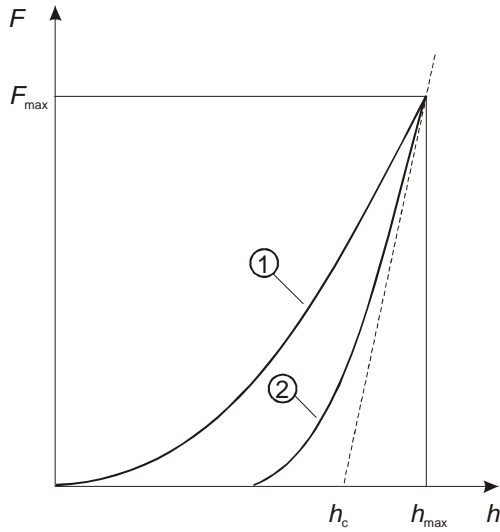


Figure 1.4 Indentation curve produced by means of the universal hardness method: 1 – load increase, 2 – load removal [15]

It is not required to determine the contact point. Both hardness definitions given in the European standard [16] deal with plastic and elastic penetration of the indenter. To calculate plastic hardness, it is essential to determine the actual penetration depth of the indenter (the permanent depth of the indentation). According to such a model, plastic hardness can be calculated using the initial unloading slope $(dF/dH)_{F_{max}}$ [17], or the Young modulus denoted as Y_{HU} .

Instrumented indentation hardness provides the ability to measure the indenter penetration h under the applied force F throughout the testing cycle and is therefore capable of measuring both the plastic and elastic deformation of the material under test [16]. The elastic portion of the deformation is referred to as elastic hardness. The depth sensing hardness method is widely used to characterize erosive wear behaviour of metal matrix composite (MMC) materials. As the erosive phenomena involve material removal due to the elastic, elasto-plastic and plastic deformation mechanisms, it can be simulated by the methods of hardness measurement.

The hardness of depth sensing has been a topic of interest in recent years. Such interest can be attributed to the number of applications of the method. Properties, such as Young's modulus, yield strength, and strain hardening exponent as well as fracture toughness of materials, can be estimated by means of continuous indentation [17].

Techniques of measuring hardness with different loads were used to simulate the impact of abrasive particles with different sizes and energy.

1.4.2 Hardness characterization

Hardness is the major, and often the only quantitative technique used for characterizing the wear resistance of the material. It is used to characterize and to predict the wear resistance of micro- and macroheterogeneous materials as well as ceramic and metallic-ceramic coatings.

It is generally believed that hardness values follow a normal distribution. For heterogeneous materials, particularly if the dimensions of the microstructural features are in the same order of magnitude as the indent depth, this is not necessarily the case [17]. Valente [18], Lin and Berndt [19] demonstrated that the Weibull hardness distribution is more appropriate for thermal spray coatings. Beckmann and Kleis

[12] used the Weibull hardness distribution function for characterization of the hardness distribution of metals.

The three-factor cumulative Weibull distribution function is given by the following equation:

$$F(H) = 1 - \exp\left(-\frac{H - H_{\min}}{H_0}\right)^m, \quad (1.5)$$

where H – measured hardness value, H_{\min} – minimal hardness value, H_0 – median hardness value, m – Weibull shape factor.

The hardness distribution function can be simplified by using the two-factor Weibull distribution. This simplification can be made for the linear regression analysis. By m values of different shape factors, the Weibull distribution approximates over other distributions. The results of the approximation are given in Table 1.7.

Table 1.7 Weibull shape factor m for the approximation of distributions [18]

$m = 1$	Weibull distribution is identical to the exponential distribution.
$m = 2$	Weibull distribution is identical to the Rayleigh distribution.
$m = 2.5$	Weibull distribution approximates the log-normal distribution.
$m = 3.6$	Weibull distribution approximates the normal distribution.
$m = 5$	Weibull distribution approximates the peaked-normal distribution.

In wear calculations, the values of $F(H)$ close to zero and one can be excluded, so that the distribution function is to be looked for in the hardness range $H' - H''$, where H' and H'' are minimum and maximum values of observed hardness.

The process of material removal during the erosive wear starts after a relatively small number of irreversible deformations, i.e. contacts between abrasive particles and the target. Therefore, the first threshold values must be exceeded, so that generally serious wear can be established. Greenwood and Williamson [22] suggested the following analytic criteria. During an indentation process, i.e. pressing a hard particle in an elastic deformable basic body, the threshold value – contact hardness H_c may be determined. From hardness H_c , the elastic contact appears, while values under it lead to irreversible deformations:

$$H_c = E \left(\frac{5\pi\rho_2 R_2 v_0^2 \sin^2 \alpha}{4E'} \right)^{0.2}, \quad (1.6)$$

where ρ_2 – density of the abrasive, R_2 – radius of the spherical indenting body, v_0 – speed of the particle before impingement, α – impact angle, E' – reduced modulus of the elasticity of contact.

The reduced modulus of elasticity of contact E' is determined by Eq. (1.8).

$$E' = \left(\frac{1 - \mu_1^2}{E_1} + \frac{1 - \mu_2^2}{E_2} \right)^{-1}, \quad (1.7)$$

where E_1 and E_2 – Young's moduli of the target material and abrasive particle, μ_1 and μ_2 – Poisson's ratios for the same materials.

If contact hardness Eq. (1.6),

$H_c > 5H'$ (HV) – plastic contact is dominant,

$H_c \leq 5H'$ (HV) – the contact is elasto-plastic,

$H_c < H'$ (HV) – the contact is elastic.

If the contact is irreversible, the process can react in two ways; it can follow one of the two alternative mechanisms: small plastic deformation or dominating brittle fracture.

If the threshold value of contact hardness, calculated according to Eq. (1.6), $H_c \leq H'$, the contact is reversible. For all values of $H_c > H'$, the contacts are irreversible. For the hardness values $H' < H_c < H''$ the area for the wear calculation $H' - H_c$ will be used and for $H_c > H''$, the area $H' - H''$ will be taken into consideration. Therefore, the irreversible effective hardness area

$$\Delta H = H_c - H' \text{ or } \Delta H = H'' - H'. \quad (1.8)$$

According to [12] the indentation depth

$$h_p = R_2 \sqrt{\frac{2\rho_2}{3H_1} \left[v_o^2 \sin^2 \alpha - \frac{4E'}{5\pi\rho_2} \left(\frac{H_1}{E'} \right)^5 \right]}, \quad (1.9)$$

and the corresponding radii of indentation

$$r_n = R[(h_p/R)_i - (h_p/R)_i^2]. \quad (1.10)$$

The effect of the particle stream is substituted by the superposition of the effects of single particles. If the kinematical dimensions of the contact are the velocity of the particle v_o and the impact angle α , then the geometrical dimensions of the contact are the radius of the contact r_n , the plastic penetration depth h_p and by brittle materials additionally the radial crack length C_r and the depth of the lateral crack h_l .

For the large contact surfaces and homogeneous materials, macrohardness can be used. With small contact surfaces or diverse materials, the local hardness of the surface must be taken into consideration, with composite materials that is always the case. The contact radii, as they appear with the wear caused by solid particle erosion, must lie, in general, in the scale of hard phase reinforcements dimensions [23].

1.4.3 Characterization of fracture toughness

The measurement of valid plain-strain fracture toughness (K_{Ic}), for the particulate reinforced metal matrix composites is an important step in the process of developing products from MMC materials. K_{Ic} is the property characterizing the resistance of a material to fracture in the presence of a sharp crack under tensile loading, where the state of stress near the crack front is a tri-axial plane strain, and the crack tip plastic region is small compared with crack size and specimen dimensions. A valid K_{Ic} value is believed to represent a lower limiting value of fracture toughness. At present there are no standard fracture toughness test procedures for the MMC, and conventional standards for metals ASTM E399 and BS 7448 are normally used. This is valid in case the K_{Ic} of the bulk material is measured.

The methodologies used to evaluate the toughness of coatings fall into one of the following methods: indentation, bending, buckling, scratching, or tensile test [24].

The Vickers indentation is a widespread technique to measure the fracture toughness of brittle materials [25] because it can be used on small samples of material not amenable to other fracture toughness tests.

Fracture toughness can be determined by measuring the post-indentation crack size. Palmqvist [26] was the first to recognize the potential of such relationship, but his treatment was purely empirical [27]. A number of formulas have been proposed for the determination of fracture toughness of a brittle material (Table 1.8).

Table 1.8 Preferred formulas for the determination of fracture toughness of WC-24Co sintered material according to Ponton and Rawlings [28]

Model authors	Equation ¹⁾	Limit of applicability
Niihara et al. [29]	$K_{1c} = 0.0089 \cdot \left(\frac{E}{HV}\right)^{2/5} \cdot \frac{P}{a \cdot l^{1/2}} \quad (1.11a)$	$2.5 \geq 1/a \geq 0.25$
Niihara et al. [30]	$K_{1c} = 0.0122 \cdot \left(\frac{E}{HV}\right)^{2/5} \cdot \frac{P}{a \cdot l^{1/2}} \quad (1.11b)$	$2.5 \geq 1/a \geq 0.25$
Shetty et al [31]	$K_{1c} = 0.0319 \frac{P}{a \cdot l^{1/2}} \quad (1.12)$	-
Laugier [32]	$K_{1c} = 0.0143 \left(\frac{E}{HV}\right)^{2/3} \left(\frac{a}{l}\right)^{1/2} \left(\frac{P}{c^{3/2}}\right) \quad (1.13)$	-
Lawn [27]	$K_{1c} = \delta \left(\frac{E}{HV}\right)^{1/2} \left(\frac{P}{c^{3/2}}\right) \quad (1.14)$	$c/a \geq \approx 2$

¹⁾ K_{1c} – fracture toughness, P – applied indentation load, E – Young’s modulus, δ – empirical constant depending on the geometry of the indenter, HV – Vickers hardness, a – indentation diagonal ($l=c-a$, where c is total crack length from the centre of the indent)

According to Lawn, et al. [27] the length c of radial cracks caused by indentation may be related to the fracture toughness K_{1c} (Eq. 1.17). For standard Vickers diamond pyramid indenter, the value of δ is taken 0.016. Crack length c can be obtained using SEM.

López Cantera, et al. [35] describe the determination of fracture toughness using Vickers indentation in WC-Co systems. Indentation testing revealed that both coatings exhibited anisotropic crack propagation and fracture toughness, crack propagation being much easier parallel to the coating/substrate interface than transverse to it.

For the coating as well as interface fracture, energy methods using extrapolation of the initial loading to the actual loading curve have been suggested [36]. This energy can be determined by the integration of the loading and unloading indentation curves. This method has been applied to thin brittle coatings. A distinct difference can be made in radial cracking, delaminating and chipping of the coating.

1.5 Objectives of the study

From the overview the following conclusions may be drawn:

- Tribological materials and coatings are typical materials of a heterogeneous structure: hard particles in a relatively soft matrix. Typical representatives of wear resistant materials are metal-matrix composites (MMC) with particulate hard reinforcements (nickel and cobalt self-fluxing alloy-based coating with carbide hard phase) and carbide-based coatings with a metal binder. Tungsten carbide (WC) based hardmetal type coatings or self-fluxing alloys based coatings containing WC, applied by the spray and fusion methods, are used. Most of the information available on the tribological properties of these alloys has been derived from laboratory tests rather than engineering applications.
- At impact wear the plastic contact is dominating by the metal-matrix of the materials and coatings and the model of plastic contact is applicable. With the hardmetal type coatings, where carbide content exceeds 50%, brittle fracture of carbide is dominating.
- Attempts have been made to correlate erosion rates with experimental parameters. The models of plastic deformation and brittle fracture have been developed to model the wear of homogeneous bulk materials.

In these models, hardness and fracture toughness emerge as the main materials parameters that control erosion; a high hardness increases resistance to plastic deformation, while high fracture toughness increases resistance to fracture. Resulting of above mentioned, the main objectives of our study were:

- Experimental determination of the important mechanical parameters of MMC materials and coatings which are used in the mathematical model of erosive wear;
- Study of erosion resistance and wear mechanisms of MMC materials and coatings with multimodal reinforcements;
- Development of a mathematical model based on the combined model of plastic deformation and brittle fracture capable of characterizing the erosive wear of multimodal MMC materials and coatings with heterogeneous structure;
- Utilization of hardness distribution of the MMC materials, presenting the results in a formalized form in Weibull distribution function and using it in erosion wear calculation of the reinforcing phase;
- Establishment of criteria for determination of hardness-toughness properties applicable for the proposed mathematical model of erosion of MMC structures.

2 MATERIALS AND EXPERIMENTAL

2.1 Studied materials

Powder metallurgy produced metal-matrix composite (MMC) materials and thermally sprayed MMC coatings were under the study. For the indentation experiments and wear calculations the following MMC material and coating with different volume fraction of hard phase served as examples:

1. Powder metallurgy produced Cr steel based metal-matrix composite material containing about 20 vol% of VC particles with sub-micron size and 20 vol % WC reinforcement with particle size about 100...300 μm .
2. Flame spray-fused (FSF) self-fluxing NiCrSiB alloy based matrix coating dispersion-strengthened with carbides, borides and silicides of Cr and Ni and consisting of about 20 vol% (WC-Co) hardmetal reinforcement with particle size about 100...300 μm .

The composition and physical-mechanical properties of different components of the abovementioned MMC materials are given in Table 2.1.

Table 2.1 Data of composite metal-matrix structures

Components	Volume fraction %	ρ_1 kg/m ³	H_1 (HV1) Gpa	E_1 GPa	μ_1
NiCrSiB alloy coating	–	8900	4.8	217	0.21
Commercial tool steel WR-6	–	7400	3.8	220	0.28
<u>Matrices</u>					
- Cr steel	71	7400	6.8	220	0.28
- NiCrSiB	80	8900	5.6	175	0.21
<u>Hard phases</u>					
- WC	29	15800	24.6	680	0.22
- WC-15Co	20	14500	14.0	560	0.23

The volume fraction of hard phase in the MMC material was determined by SEM micrographs using the image analysis program Image Pro. The microstructure of the material is given in Fig 2.1 and that of the coating in Fig 2.2. Material and coating porosity, determined by the image analysis, was less than 0.8%.

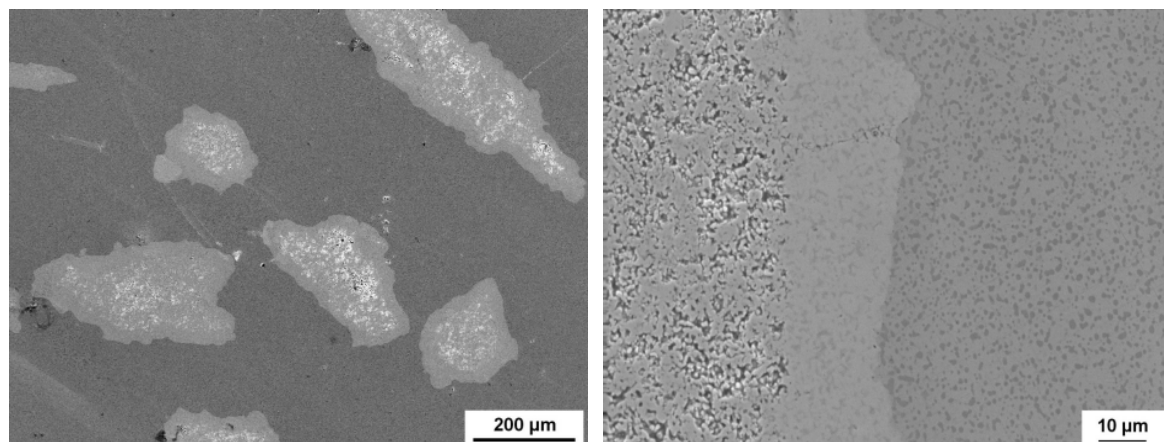


Figure 2.1 Microstructure of the PM MMC material based on the Cr steel matrix with VC micro particles and WC reinforcement

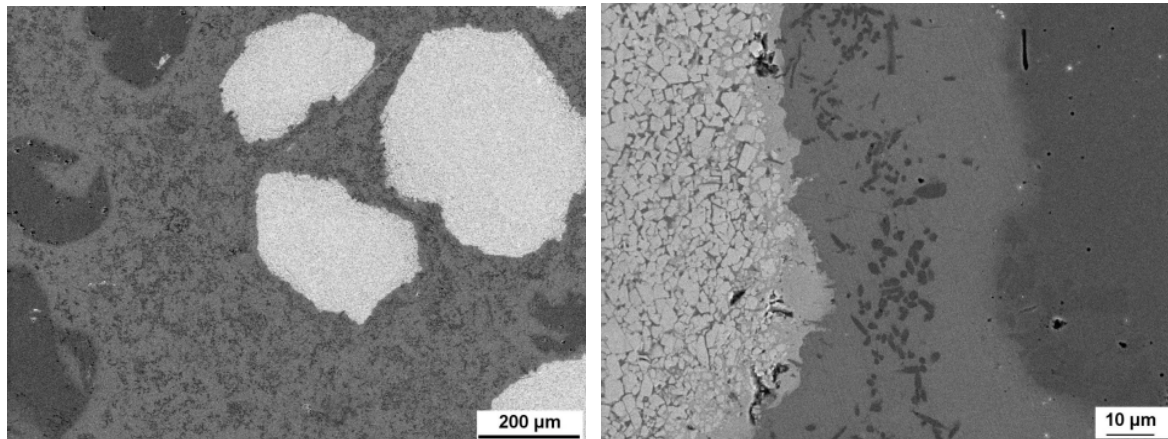


Figure 2.2 Microstructure of the FSF coating based on the self-fluxing NiCrSiB alloy with recycled WC-Co hardmetal reinforcement

2.2 Indentation method for the characterization of materials

2.2.1 Hardness measurements

Hardness was used to describe qualitatively the mechanical response of the wear surface. For that purpose measurements in different hardness scales were used:

- a) measurements of materials hardness in the macrohardness range according to EVS-ISO 6507 using Vickers hardnessmeter (Indentec 5030 SKV) and a load of 294.2 N (30 kgf). The indents were performed with a regular spacing of 1 mm
- b) measurements of materials hardness in the microhardness range, using instrumented hardnessmeter (Zwick Z2.5) with Vickers indenter and load 9.8 N (1.0 kgf) and microhardnessmeter (Micromet 2001) with Vickers indenter and a load of 0.98 N (0.1 kgf). In microhardness measurements, spacing between indents was selected 0.5 mm. Instrumented hardness (HU) measurements were carried out by standard procedures [20]. The load of 9,8 N was applied to the specimen in 7 s. The indentation was performed under load control. The dwell time of 3 s was used to suppress the effect of elastic recovery. The unloading time was 3.5 s. Spacing between indents was kept 1.0 mm. The elastic modulus of the material was determined from the slope of the unloading part of the load – indentation curve obtained using the instrumented hardness method
- c) measurements of material (reinforced with VC submicronical particles) in nanohardness range using Nanoindenter XP with Berkovich indenter and at load range ~ 1 N (0.1 kgf). The equipment for nanoindentation does not rely on readings of residual indents dimension, but rather on precise loading and recording of the indentation depth. However, the small indentation depth causes artefacts due to micro scale surface roughness, tip geometry and elasticity. In the present study, hardness was measured at the indentation depth of 100 nm. Spacing between indents was 10 μm .

Altogether, a minimum of 100 measurements was performed. Hardness measurement results at different hardness scales were then mathematically treated.

In view of the fact that the average hardness in the contact area is varying monotonous, the Weibull cumulative distribution function, presented in the form shown in Fig. 2.3, was used.

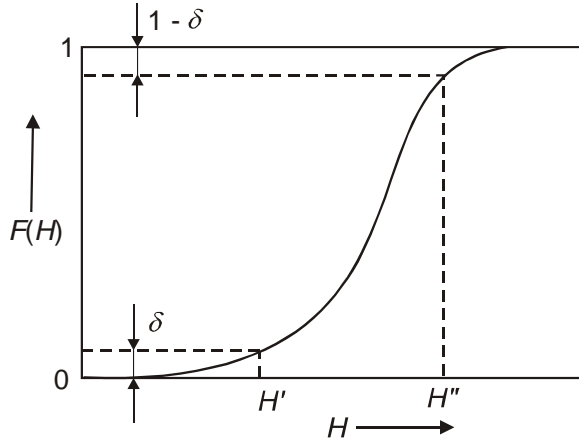


Figure 2.3 Hardness distribution function of a material

For wear calculation, the values of $F(H)$ around zero and one were excluded, so that the distribution function was to be looked for in the area $\delta \leq F(H) \leq 1 - \delta$. In our experiments, at wide hardness range up to ten values of hardness (5 maximum and 5 minimum ones) were excluded. Therefore, the hardness area $H' \dots H''$ was observed only. The hardness $\Delta H = H'' - H'$ was divided into $n = 6$ intervals. The mean values of intervals and the length of an interval $\Delta H/n$ were calculated. On the basis of experimental data, the Weibull hardness distribution function parameters m and H_0 were found according to Eq. (2.1).

$$F(H) = 1 - \exp\left(-\frac{H}{H_0}\right)^m \quad (2.1)$$

2.2.2 Determination of fracture toughness and fracture probability

The fracture toughness of single carbide or WC-Co hardmetal particles as reinforcements in the MMC material was determined by means of Vickers indentation. It is possible to relate the toughness K_{1c} directly to postindentation crack size [28]. The surface length of the arrested cracks, emanating from the corners of the Vickers indentations (Fig 2.4), was related to the fracture toughness of the material via relationships given in Table 1.8.

$$K_{1c} = 0.0122 \left(\frac{E}{HV}\right)^{2/5} \frac{P}{a \cdot l^{1/2}} \quad (2.2)$$

As the fracture behaviour of carbides is extremely sensitive to surface preparation, it was adequately polished using diamond as abrasive. The indents were produced using Vickers hardness tester. A load of 1.0 N was found to be sufficient to cause the Palmqvist cracks in the length of tolerable limits.

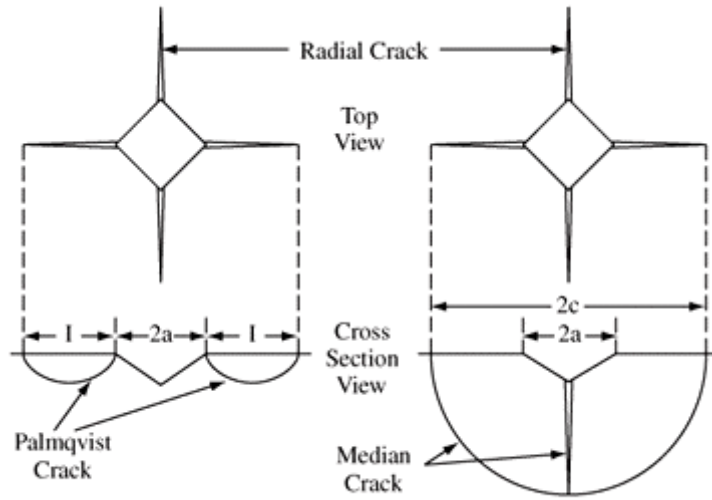


Figure 2.4. Indentation fracture pattern for Vickers geometry

The cracks were measured in carbide particles of average size. For measuring purposes, only particles with no visible defects (cracks, inhomogenities etc) were used. In every carbide only one indent was done. The length of the radial cracks was measured using SEM. The crack length from the centre of the indent, denoted c , is the sum of crack length from indent corner l and half the indent diagonal length $2a$. Hence, $c = a + l$.

The fracture probability P (probability of a fracture or crack initiation) was determined emanating from the normal force F_n caused by the particle in the contact, the hardness H_1 and fracture toughness K_{1c} . Thus, for the contacts that cause crack initiation and the total number of irreversible contacts, two dimensionless parameters, such as the value of $F_n \cdot H_1^3 / \text{const} \cdot K_{1c}^4$ and probability P , were found. In addition, it is assumed that between these dimensionless parameters, the Weibull distribution is valid and expressed by the cumulative probability function

$$P = F(F_n) = 1 - \exp \left\{ - \left(\frac{F_n \cdot H_1^3}{\text{const} \cdot K_{1c}^4} \right)^m \right\} \quad [2.3]$$

with parameters $(\text{const} \cdot K_{1c}^4) / H_1^3$ and m . According to [29], the appearing constant can obtain values from $(0.5 - 1.5) \cdot 10^3$.

2.3 Erosion testing

2.3.1 Erosion tester

Erosion resistance of materials and coatings was determined with the centrifugal accelerator CAK-3m in accordance with the standard method [30]. The principal scheme of the tester is provided in Fig. 2.5.

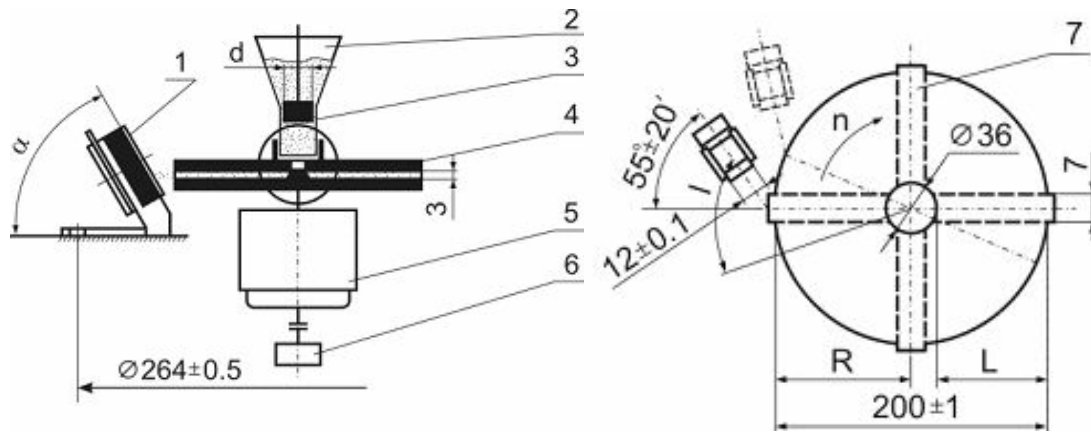


Figure 2.5. Abrasive erosion tester for testing materials in abrasive particle jet: 1 – specimen, 2 – erodent hopper, 3 – shield, 4 – rotor, 5 – drive motor, 6 – rotation speed gauge, 7 – radial channels.

Specimens (25 x 15 x 4...5 mm) were spark erosion cut and ground with sufficient water cooling to the required thickness. Before the test, the specimens were subjected to the wear-in process in the same conditions. The weight loss for each material tested in the given conditions (particle velocity, impact angle) was calculated as average weight loss of three individual wear specimens. Based on the weight loss of abraded specimen, the volumetric wear rate (loss of volume per one kilo of erodent in mm³/kg) was calculated. The relative erosion resistance ε was calculated as the ratio of the volumetric wear rates of the reference material I_v^r (0.45% C steel, 200HV) and the studied experimental material or coating I_v^e .

$$\varepsilon = I_v^r / I_v^e \quad (2.4)$$

The maximal particle size of the erodent which can be used in the centrifugal accelerator CAK-3m can be up to 1 mm. To investigate the impact wear resistance of the material with bigger particle size a modified disintegrator DESI 15 was used. The principal scheme of the disintegrator is given in Fig. 2.6. For that purpose the rotor blades were redesigned as specimen holders. The specimens with same dimensions as in the centrifugal accelerator CAK-3m were used in impact testing. The impact angle and particle velocity depends on the relative rotational speed of inner and outer rotors of the disintegrator. In our tests, the relative speed was selected to provide impact angle 85...90° at particle velocity of 80 m/s.

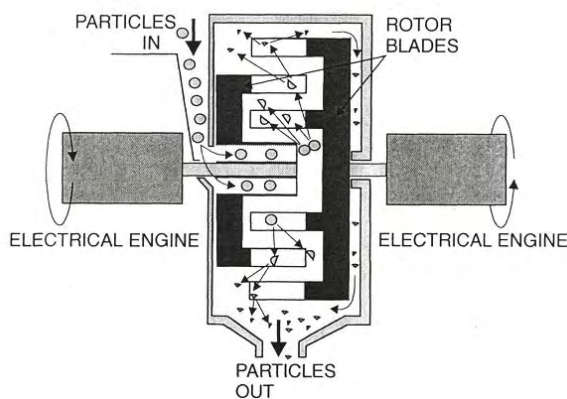


Figure 2.6 Principal scheme of impact wear tester

2.3.2 Used erodents

For erosion tests, quartz sand with two different particle sizes was used as an erodent. In dust erosion tests, quartz sand dust was used, manufactured by multiple milling of quartz sand in the laboratory disintegrator milling system DSL-175. The physical and mechanical properties of the erodents are given in Table 2.2.

Table 2.2 Physical and mechanical properties of the erodents

Composition	SiO ₂
Mean particle size d_m , μm	
quartz sand	100...300
quartz sand dust	10...30
Hardness HV, GPa	11.5
Density ρ_2 , kg/m ³	2200
Elastic modulus E_2 , GPa	90
Fracture toughness K_{Ic} , N/mm ² ·m ^{0.5}	0.7

Erodent particles morphology and also size were examined using the scanning electron microscope (SEM) JEOL JSM-840A. The SEM images of the used erodents are given in Figure 2.7 (a) and (b). The particle size distribution of the erodent was investigated by the laser diffraction method, using the laser particle analyzer Analisette 22 Compact. The particle size distribution is given in Figure 2.8 (a) and (b).

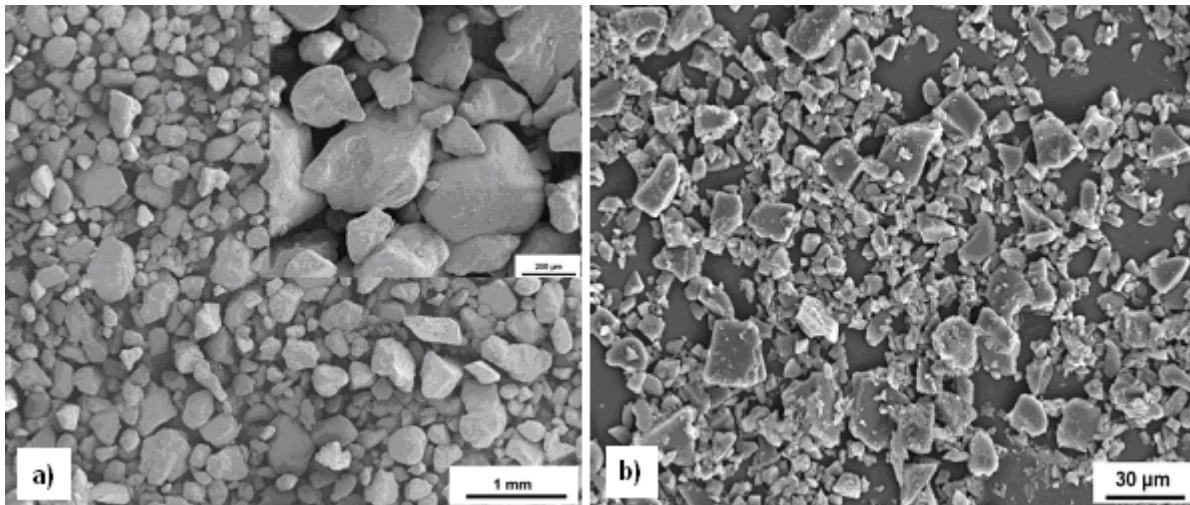


Figure 2.7 SEM images of quartz sand (a) and quartz sand dust (b) used in erosion tests

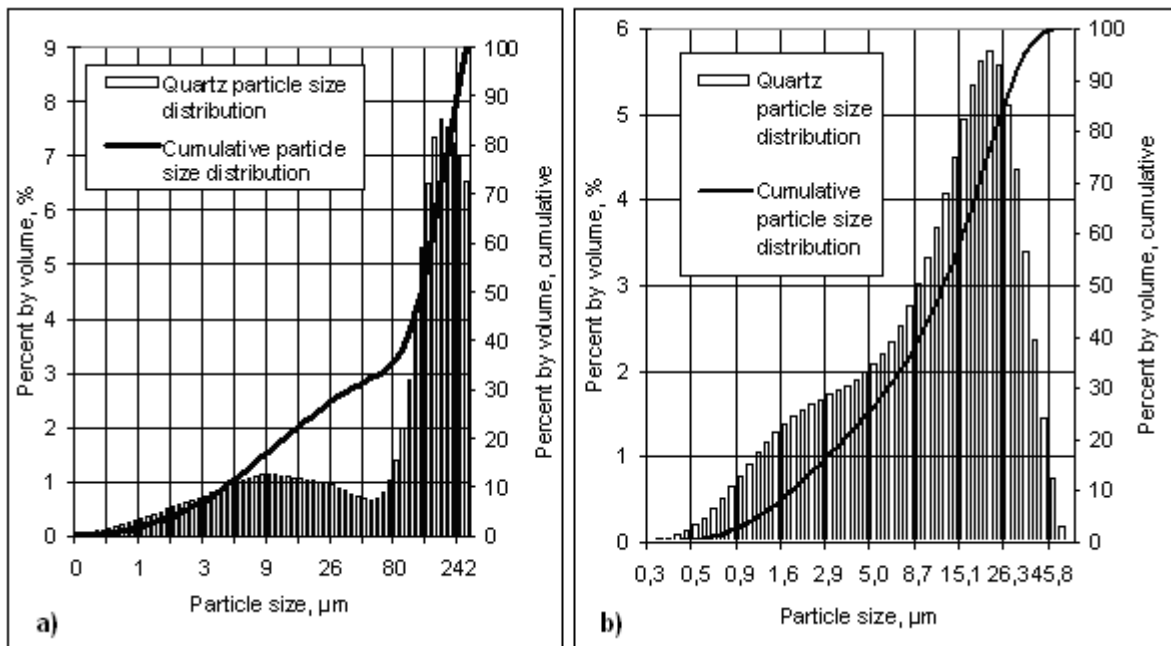


Figure 2.8 Particle size distribution of quartz sand (a) and quartz sand dust (b)

In impact wear testing granite gravels with average particle size of 2.8...5.6 mm were used. The granite gravels are depicted in Fig. 2.6 (a) and the results of sieve analysis are given in Fig. 2.6 (b).

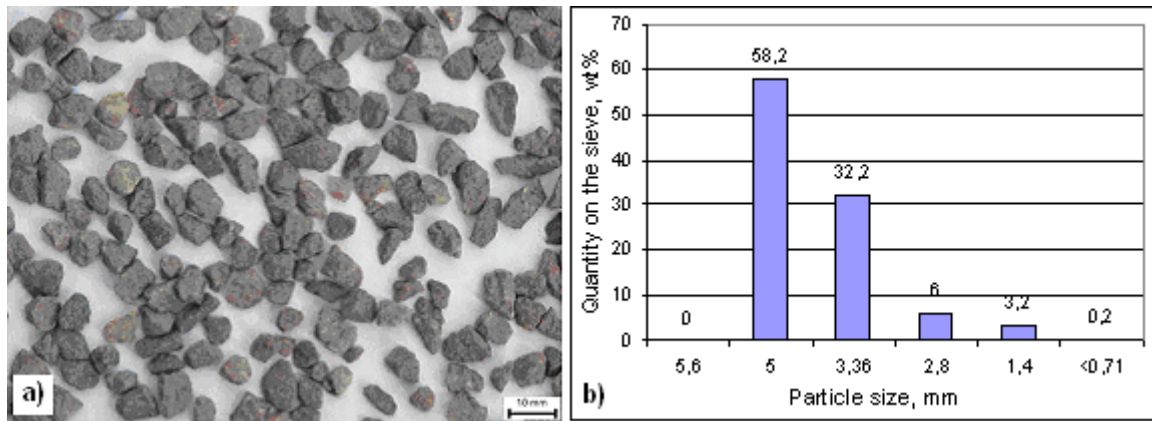


Figure 2.5 Image of granite gravels (a) and particle size distribution by sieve analysis (b)

2.3.3 Study of worn surfaces

The study of worn surfaces comprised an analysis of SEM images of surface and the results of the Vertical Scanning Interferometry (VSI), using the optical surface profilometer WYKO. Using the profilometer, the vertical scanning resolution was 3 nm, resolution in the direction of axes x and y was 0.5 μm . The SEM study was carried out using JEOL JSM-840A. For the study of worn surfaces acceleration voltage of 15 KV was usually applied for observation. Probe current was approximately 10^{-9} A. Secondary electrons were used for the image. The working distance was in between 15...24 mm.

3 CHARACTERIZATION OF POWDER COMPOSITE MATERIALS AND COATINGS USING INDENTATION

3.1 Hardness characterization of the MMC material with multimodal reinforcements

Depending on the microstructure of the powder metallurgy Cr–steel based metal-matrix composite material (Cr–steel+20 vol% VC)+ 20 vol % WC) with multimodal reinforcements (sub-micronical VC carbides and WC particle sizes of some hundreds of microns), different hardness measurements (macro-, micro- and nanoscale) for the evaluation of hardness distribution of the MMC material were carried out.

Hardness measurements in the *macrohardness* range of the MMC material with Vickers hardness tester at a load of 294 N were performed. Hardness values varied from 5925 to 6927 MPa. The results were divided into six groups. The hardness intervals and mean values of the intervals are given in Table 3.1. The Weibull distribution function Eq. (11) was found the most suitable mathematical function to describe the distribution of hardness values. Using the last square method, the shape parameter m and median hardness H_0 were found 3.0 and 6.30, respectively. Figure 3.1 demonstrates the agreement of experimental and calculated distribution functions.

Table 3.1 Hardness intervals and mean hardness values of the MMC material using macrohardness HV30

Hardness HV30, MPa		Indentation diagonal $d_m, \mu\text{m}$
Interval	Interval mean hardness	
5 925-6 090	6 011	301.3
6 090-6 257	6 180	297.2
6 257-6 424	6 349	293.3
6 424-6 590	6 519	289.5
6 590-6 757	6 688	285.9
6 757-6 927	6 858	282.4

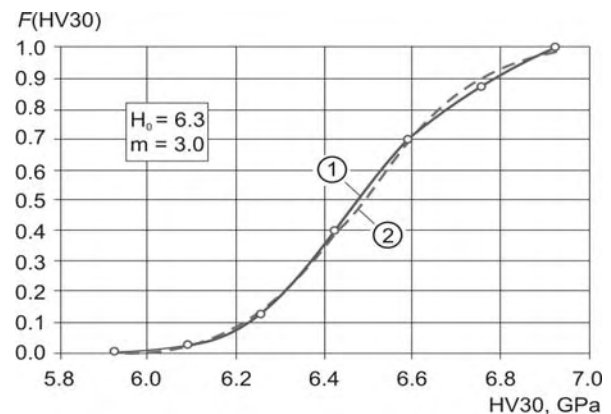


Figure 3.1. Experimental (1) and theoretical (2) hardness HV30 distribution of MMC material

Hardness measurements in the *microhardness* range of the MMC material with the universal hardnessmeter Zwick 2.5 at a load 9.8 N and microhardnessmeter Micromet 2001 at a load of 0.98 N were performed in regular intervals of 0.5 mm. The hardness values taken into consideration varied from 4073 to 12 336 and from 3088 to 22 890 MPa at universal hardness HU1 and microhardness HV0.1 respectively. The total hardness range was divided into $n = 6$ intervals. The six intervals and their mean values are given in Tables 3.2 and 3.3. For the experimental and theoretical microhardness distribution functions are given in Fig. 3.2 and 3.3, the median hardness H_0 and shape parameter m were found.

The mean values of hardness intervals of universal hardness of MMC measured by the depth sensing hardnessmeter Zwick 2.5 at a load of 9.8 N varied from 4762 to 11 650 MPa (Table 3.2).

Table 3.2 Hardness intervals and mean hardness values using universal hardness HU1

Hardness HU1, MPa		Indentation diagonal $d_m, \mu\text{m}$
Interval	Interval mean hardness	
4073-5450	4762	62.5
5450-6827	6140	55.0
6827-8204	7517	49.5
8204-9581	8895	46.5
9581-10 951	10 273	42.5
10 951-12 336	11 650	40.0

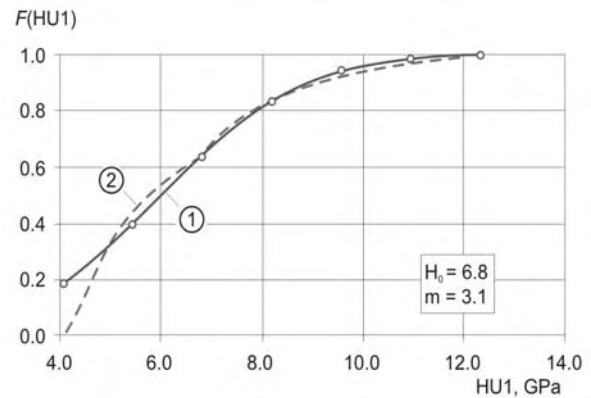


Figure 3.2. Experimental (1) and theoretical (2) universal hardness (HU1) distribution of MMC material

As follows from Fig. 3.2 there exists a good coincidence between experimental HU1 and the theoretical values. The best coincidence of the experimental and the theoretical Weibull distribution values was observed with median hardness $H_0 = 6.8$ and shape parameter $m = 3.1$.

The mean values of hardness intervals of microhardness varied from 4540 to 19 040 MPa (Table 3.3).

Table 3.3 Hardness intervals and mean hardness values of MMC material using microhardness HV 0.1

Hardness HV0.1, MPa		Indentation diagonal $d_m, \mu\text{m}$
Interval	Interval mean hardness	
3 080-5 990	4 540	20.2
5 990-8 890	7 440	15.8
8 890-11 790	10 340	13.4
11 790-14 690	13 240	11.8
14 690-17 590	16 140	10.7
17 590-20 490	19 040	9.8

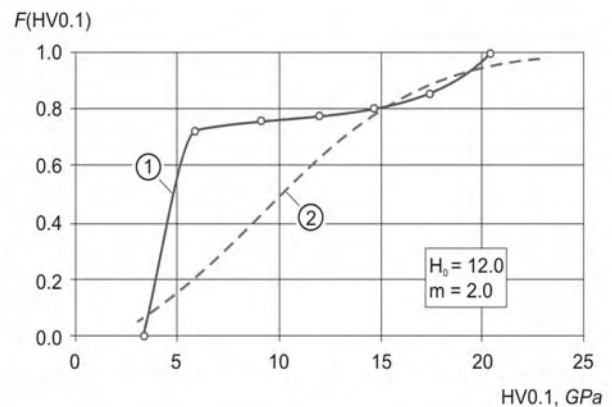


Figure 3.3. Experimental (1) and theoretical (2) microhardness (HV0.1) distribution of MMC material

The best coincidence of the experimental and theoretical two-parametrical Weibull distribution values was observed with median hardness $H_0 = 12$ and shape factor $m = 2.0$. The coincidence between theoretical and experimental microhardness HV0.1 distribution curves can be witnessed only at higher hardness values (Fig. 3.3).

An analysis of the microhardness HV0.1 test results was carried out, the measurements were divided into two distinctive groups: 67 measurements between 3080 and 5722 MPa (metal-matrix) and 23 measurements between 8818 MPa and 20 490 MPa (hard phase).

Later, the second group of hardness values (from 8818 to 20 490 MPa, hardness of hard phase) was divided into six hardness intervals. The length of the interval was 1954 MPa. The hardness intervals and the mean value of the interval are given in Table 3.4 and hardness distribution functions of hard-phase in Fig. 3.4. The median hardness H_0 and shape parameter m were found.

Table 3.4 Hardness intervals and mean hardness values of hard phase

Hardness HV0.1, MPa		Indentation diagonal $d_m, \mu\text{m}$
Interval	Interval mean hardness	
8818-10 772	9795	13.8
10 772-12 726	11 749	12.6
12 726-14 680	13 703	11.6
14 680-16 634	15 657	10.9
16 634-18 588	17 611	10.3
18 588-20 543	19 565	9.7

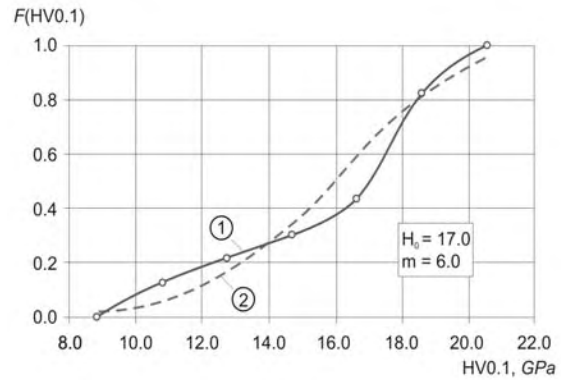


Figure 3.4. Experimental (1) and theoretical (2) microhardness (HV0.1) distribution of hard phase of MMC material

The best coincidence of the experimental and theoretical two-parametrical Weibull distribution values of microhardness of hard phase was observed if $H_0 = 17.0$ and $m = 6.0$ (Fig. 3.3)

Hardness measurements in the *nanohardness* range of the MMC material were done using the MTS nanoindentation tester and Berkovich indenter. Tests were performed under load control. The limit was set on 100 nm, after achieving the required indentation depth, the load was removed.

The measured hardness values were in the range of 1380 to 10 010 MPa. The total hardness range was divided into $n = 6$ intervals: 1380-2820 (with the mean value of interval 2100), 2820-4260 (3540), 4260-5070 (4980), 5700-7130 (6420), 7130-8570 (7850) and 8570-10 010 (9290) MPa. The length of an interval $\Delta H/n = 1440$ MPa.

The median hardness H_0 and shape parameter m values of the nanohardness distribution function were calculated. Fig. 3.5 illustrates the nanohardness distribution function. The best coincidence of the experimental and theoretical Weibull distribution values was observed if median hardness $H_0 = 2.4$ and shape parameter $m = 4.5$.

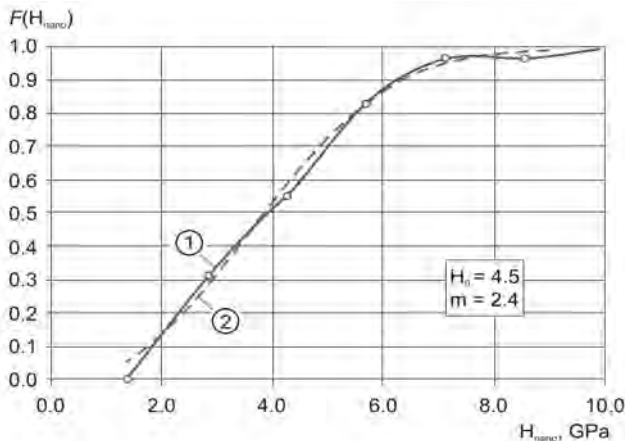


Figure 3.5 Experimental (1) and theoretical (2) nanohardness distribution of MMC material

The indentation hardness measurements of MMC material carried out using different load scales differed from each other in order of magnitude, showed that the minimum and maximum hardness values measured on the same sample may differ significantly, depending on the used hardness scale. The conclusion from hardness measurements is the following – indentation methods and parameters selection are based on a presumption that the wear marks caused by the erodent and the indents produced by the hardness measurement procedure must have similar geometry, e.g. similar depth and/or diameter.

3.2 Hardness characterization of MMC coating

The indentation hardness measurements of the flame spray fused (FSF) NiCrSiB+20 vol% (WC-Co) coating were obtained using a depth sensing indentation equipment Zwick Z2.5. An indentation load of 9.8 N was applied. The hardness of the area from 570 to 7855 MPa was taken into consideration. The hardness range (Eq. (1.6)) was divided into $n = 6$ intervals. The length of an interval $\Delta H/n = 1214$ MPa. The hardness intervals and their mean values are given in Table 3.5. The theoretical and experimental hardness distribution functions are shown in Fig. 3.6.

Table 3.5 Hardness intervals and mean hardness values of MMC coating

Hardness HU1, MPa		Indentation diagonal d_m , μm
Interval	Interval mean hardness	
570-1784	1177	127.0
1785-2998	2392	88.0
2999-4212	3606	72.0
4213-5426	4820	62.0
5427-6640	6034	55.0
6641-7855	7248	50.5

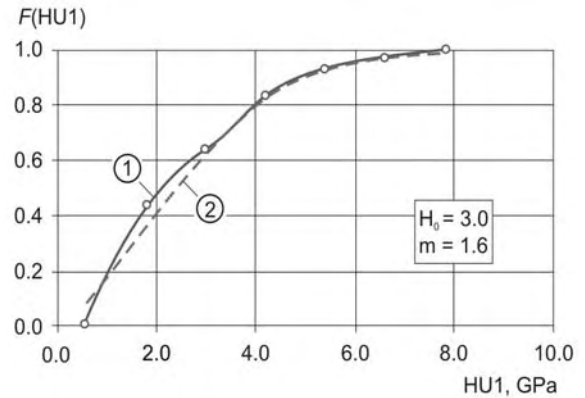


Figure 3.6 Experimental (1) and theoretical (2) hardness distribution (HU1) of MMC coating

The experimental and theoretical values of the hardness HU1 distribution function were calculated. The values for H_0 and m were found by the numerical extrapolation of the function. The best coincidence of the experimental and theoretical Weibull distribution values was observed if median hardness $H_0 = 3.0$ and shape parameter $m = 1.6$. As it follows from Fig. 3.6, there exists a good coincidence of experimental and theoretical values of HU1.

3.3 Fracture toughness and fracture probability of the hard phase

The fracture toughness of single carbide particles with a size of some hundreds of μm was determined using Vickers indentation method (also referred to as Palmqvist method) [28]. In the measurements of indents (Fig. 3.6 a) and radial cracks caused by indentations (Fig. 3.6 b) SEM was used.

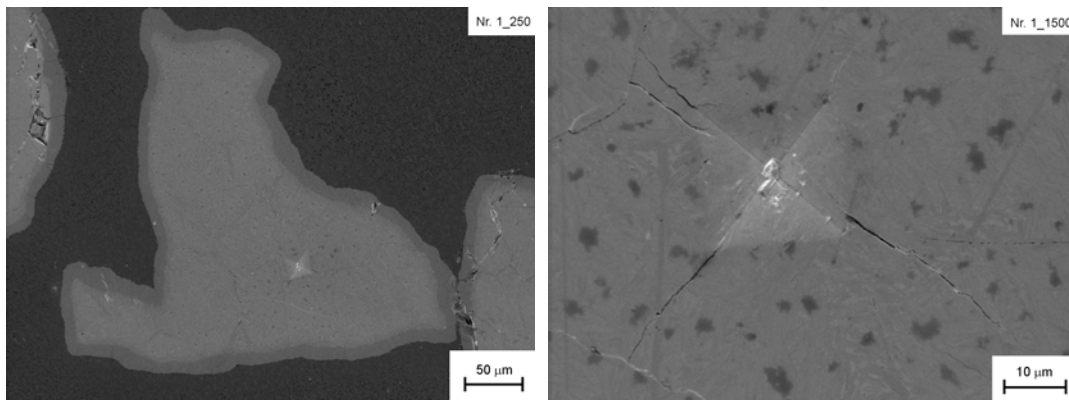


Figure 3.6. Indentations on the WC carbide particle with different magnifications

The fracture toughness was calculated according to Eq. (2.2). Table 3.5 shows the results of the calculations of fracture toughness of the WC and probability of fracture under static indentation conditions at load 10 N. Numeric analysis of the probability P value shows, it to be highly dependent on K_{Ic} .

Table 3.5 Results of fracture toughness and fracture probability calculations of WC in the MMC material (Cr steel-VC)+WC

H_1 , GPa	K_{Ic} , MPa·m ^{0.5}	$K_{Ic}^4/H_1^3 \cdot 10^{-3}$, N	Probability p at HV0.1
12.5	4.4	0.1919	0.94
17.0	2.8	0.0125	0.17

Attempts were made to determine the fracture toughness K_{Ic} value of the reinforcing phase – hardmetal of the MMC coating. Using different loads several Vickers indents (Fig. 3.7) were produced in the WC-Co hardmetal particles with size of 100...300 μm . The load varied from 0.98 N to 49 N and diagonal of the indents varied from 5 to 150 μm . Due to the relatively high toughness of the hardmetal-type reinforcement no radial cracks were produced. Higher loads resulting in the fracture of the hardmetal particles were not applicable. As the result, K_{Ic} value from the literature (about 12 MPa·m^{0.5}) was used in erosion wear calculations.

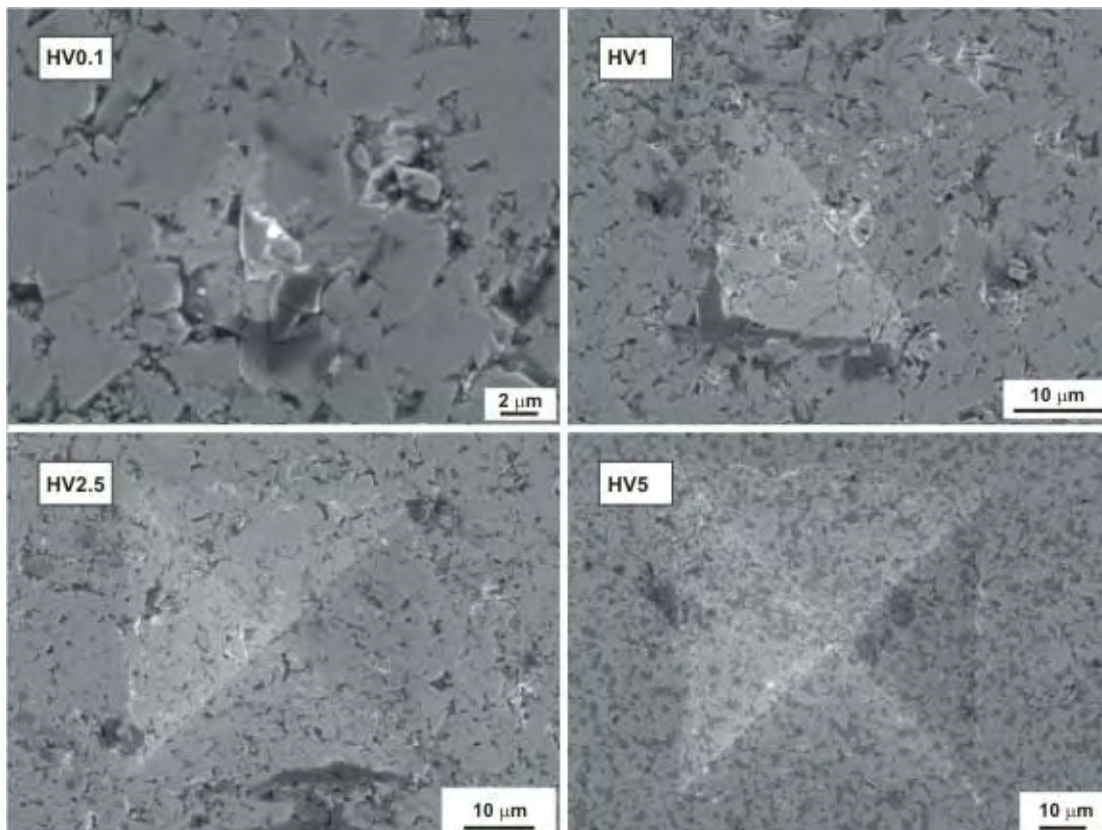


Figure 3.7. Vickers indents in the hard phase of MMC coating

4 EROSION RESISTANCE AND WEAR MECHANICS OF POWDER MATERIALS AND COATINGS

4.1 Erosion resistance of MMC materials

The wear performance of metal matrix composite materials reinforced with carbides was tested in different conditions of solid particle erosion.

Target materials for erosion testing were MMC materials with three different reinforcing phases. The metal matrix phase of the powder composites was chromium-alloyed steel with Cr content 5.25% to increase corrosion resistance. The MMC materials consisted of VC dispersion-strengthened steel-based matrix and carbides of WC, TiC or NbC. Hardox 400 and AISI 313 steels were used as reference materials. Table 4.1 provides data on the studied materials.

Table 4.1 Tested PM MMC materials

Material	Matrix	Hard phase, vol %
A	(Cr steel)+VC	TiC, 18.8 %
B	(Cr steel)+VC	WC, 18.5 %
C	(Cr steel)+VC	NbC, 19.3 %

The composition and properties of MMC materials are described in detail in [V]. Two types of quartz sand erodents were used: normal quartz sand 100...300 μm and quartz sand dust 10...30 μm . All the materials were tested at particle velocities 50 and 20 m/s and at three impact angles (30°, 60° and 90°). The volumetric erosion rate (mm^3/kg) was determined. The results of erosion tests are given in Fig. 4.1–4.4.

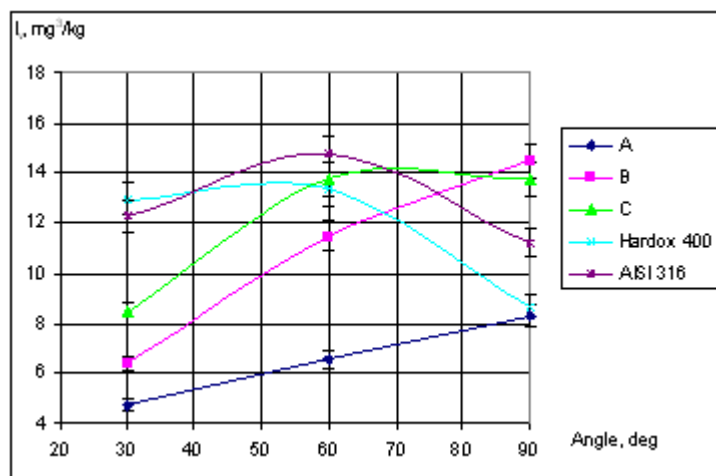


Figure 4.1 Dependence of erosion rate of MMC materials on the impact angle ($v = 50$ m/s, erodent - quartz sand 100...300 μm)

At solid particle erosion, in most cases the tested materials suffered the highest erosion rates at the impact angle of 90° at both studied velocities. This behaviour is typical of brittle materials. Both reference materials (Hardox 400 and AISI316) suffered the highest erosion rates at impact angles of 60° at the velocity of 50 m/s and at the impact angle of 30° at lower velocities. This can be explained by a relatively high toughness and fine microstructure of these steels. Comparison of the tested MMC materials revealed that the highest relative wear resistance at the particle velocity of 50 m/s was demonstrated by material A (reinforced with TiC), followed by material B (with WC). At the impact angles of 30°, the wear resistance of material A was about 2.5 times higher than the erosion resistance of AISI 316.

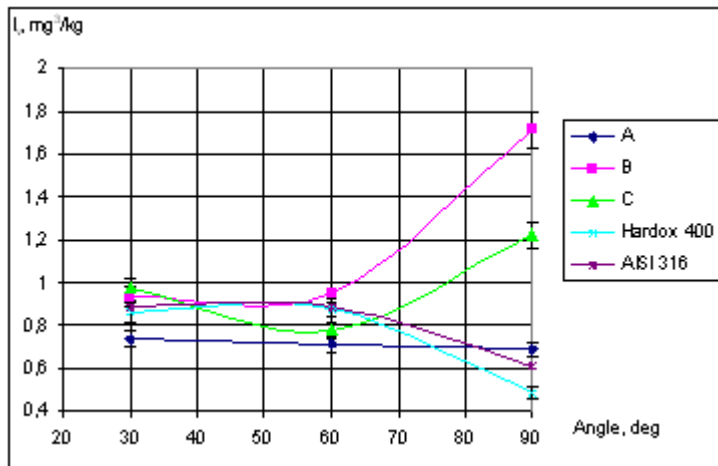


Figure 4.2 Dependence of erosion rate of MMC materials on the impact angle ($v = 20$ m/s, erodent – quartz sand 100...300 μm)

To investigate the influence of the particle size on the wear behaviour of the PM MMC material, an erosion test was conducted with quartz sand dust. In these tests, six kilos of abrasive were used. The velocity selected was 80 m/s, mainly due to the fact that a measurable wear was difficult to obtain at lower particle velocities. The tests were performed for material B only. The results are given in Fig. 4.3.

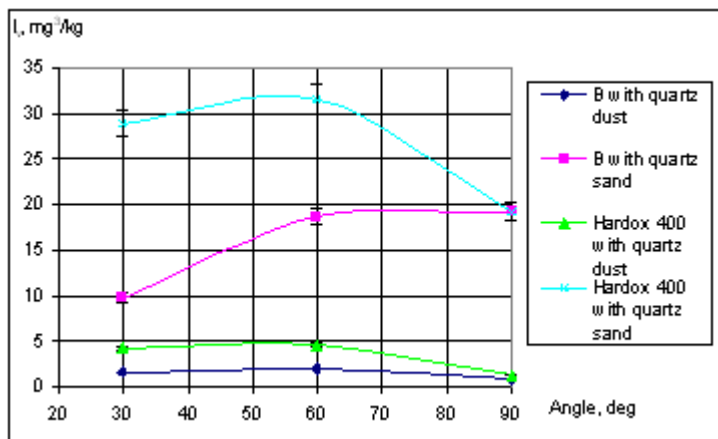


Figure 4.3 Dependence of erosion rate of MMC materials on the impact angle with different erodents (erodent – quartz sand 100...300 μm and dust 10...30 μm , $v = 50$ m/s)

To study the influence of particle size on the impact wear at a larger range of abrasive particles, the disintegrator based equipment DESI was used for particle acceleration. As an abrasive and at the same time a material to be treated, granite gravels with a particle size of 2.8...5.6 mm and hardness of 1050...1100 were used. So in the experiments the mean particle size varied from the range of a few tens of μm up to several thousands of μm . The test was conducted only with material B ((Cr steel+VC)+WC). Estimated impact angles were 80...90°. Particle velocity was in the range of 75...80 m/s. The weight loss of the specimens was measured and volumetric wear rate was calculated: 22.5 mm^3/kg for PM MMC material B (average of 4 specimens) and 66.0 mm^3/kg for Hardox 400 eroded in the given conditions.

The sensitivity of the material B to particle size is demonstrated in Fig 4.4. In the experiments the mean particle size varied in the range of a few tens up to several thousands of μm .

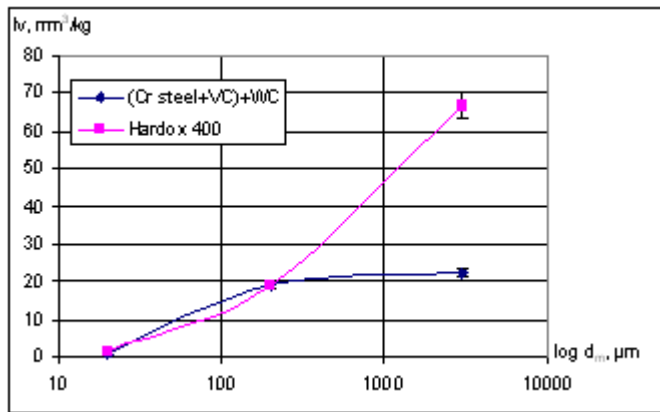


Figure 4.4 Dependence of the erosion rate of material B on the erodent particle size at high energy impact wear (erodent – granite gravels 2.8...5.6 , quartz sand 100...300 μm and dust 10...30 μm , impact angle 90° , $v = 80$ m/s)

It can be seen that the MMC material is less sensitive to the increase of the erodent size compared to the reference material Hardox 400. It has to be noted that the results are not directly comparable, as the tests with larger particles were conducted at lower velocities and with different abrasive hardness.

4.2 Erosion resistance of MMC coatings

The erosion wear of flame-spray fused (FSF) and high-velocity oxy fuel-sprayed (HVOFS) coatings was tested. The results of the erosion wear tests are given in [IV].

We used hardmetal powders WC-17Co and WC-10Co-4Cr (agglomerated and sintered), specified as Tafa 1343V and 1350M and self-fluxing NiCrSiB alloy powder, specified as Tafa 1275H (Tafa Inc.) for HVOF spraying. The studies of coating properties are described in [III and IV]. The erosion rate and/or relative wear resistance are given in Tables 4.1 and 4.2.

Table 4.1 Erosion rate and relative wear resistance ε of HVOF sprayed coatings ($v = 80$ m/s, quartz sand 100...300 μm)

Coating material	Erosion rate, mm^3/kg		Relative wear resistance ε	
	$\alpha = 30^\circ$	$\alpha = 90^\circ$	$\alpha = 30^\circ$	$\alpha = 90^\circ$
Tafa 1343V	2.6	12.3	10.8	2.6
Tafa 1350M	6.2	10.1	2.9	1.4
Steel C=0.45%	28.3	31.8	1.0	1.0

In the case of low and medium impact angles, the erosion rate decreases with an increase of coating hardness, whereas the mechanism of microcutting is prevailing. By coatings with higher hardness (HVOF sprayed hardmetal coating of WC-17Co with hardness of 1300 HV1), an increase in coating hardness causes a decrease of erosion resistance at normal impact and a direct fracture occurs.

Table 4.2 Relative wear resistance of NiCrSiB alloy based coatings deposited with different methods ($v = 80$ m/s, quartz sand 100...300 μm)

Coating material	Method of deposition	Relative wear resistance ε	
		$\alpha = 30^\circ$	$\alpha = 90^\circ$
NiCrSiB (Castolin 12495)	FSF	1.3	0.6
NiCrSiB+20vol%(WC-Co)	FSF	2.1	0.5
Metco 16C+30wt%(WC-Co)	LSF	1.6	0.3
NiCrSiB (Tafa 1275H)	HVOFS	0.6	0.3

The wear resistance of NiCrSiB sprayed and fused coatings is low ($\varepsilon < 1.0$); the best coating was NiCrSiB-based coating with recycled hardmetal reinforcement ($\varepsilon > 2.1$ at $\alpha = 30^\circ$).

At high impact angle, erosion resistance of all coatings was lower than that of the reference material – steel 0.45% C.

Erosion tests with a flame-spray fused self-fluxing NiCrSiB alloy based composite coating containing about 20 vol% (WC-Co) hardmetal were carried out at different impact angles with quartz sand of size 100...300 μm . The results are given in Fig 4.5.

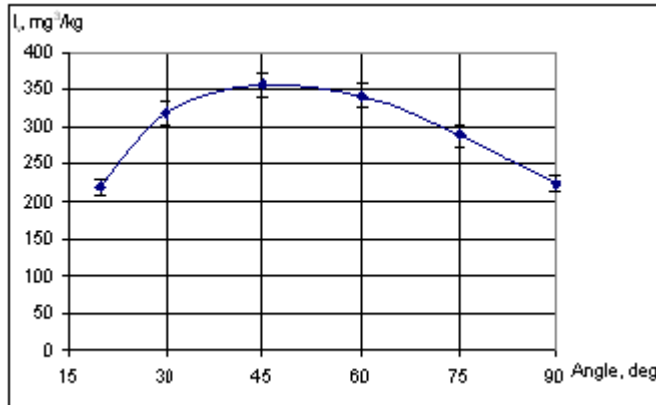


Figure 4.5 Influence of impact angle on the erosion rate of FSF MMC NiCrSiB + 20 vol%(WC-Co) coating

The following conclusions can be drawn from the erosion tests with coatings: if the erosion rate of sprayed coatings (hardmetal and self-fluxing alloy based) is maximum at high impact angles, then with fused coatings (such as pure NiCrSiB and NiCrSiB-(WC-Co) composites) it is so at medium impact angles (30...60°).

4.3 Wear mechanisms

To reveal the material behaviour in the conditions of solid particle erosion, a SEM study was conducted.

The wear surfaces of the PM MMC material (FeCr+VC)+(WC) were investigated using SEM JEOL-840A at different magnifications.

The surfaces presented in Figs 4.6 and 4.7 were subjected to erosion with quartz sand particles of 100...300 μm at the velocity of 80 m/s.

In Fig. 4.6, the characteristic features of erosion at low impact angles ($\alpha=30^\circ$) can be observed: hard quartz particles intrude into the matrix surface, forming grooves and craters. As the surface of tungsten carbide is relatively resistant to the impact of erodent particles of this size and velocity, a fracture may occur mainly due to the following two mechanisms:

- the carbide skeleton becomes vulnerable after the matrix has been removed due to microcutting, the metal matrix around the large carbide particles will be removed after a number of impacts and the carbide particle separates finally from the surface of the material;
- the direct fracture of the carbide particles after a number of impacts. Particles of a size comparable to the carbides and with sharp edges cause separation of smaller splinters from the carbide grain after multiple strikes. The surface of the carbide becomes uneven and rough.

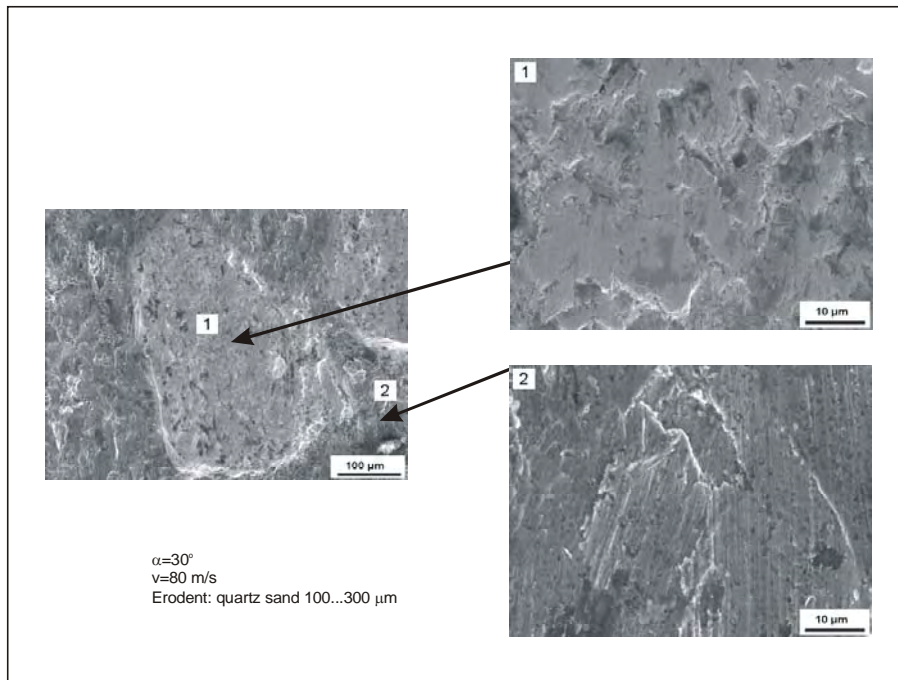


Figure 4.6 SEM images of the eroded surfaces of the PM MMC material (Cr steel+VC)+(WC).

The typical SEM image of the surface eroded by quartz sand at normal impact angle can be seen in Fig. 4.7. In this case the marks of plastic deformation of the matrix surface can be seen. Erodent particles have produced more craters instead of grooves. The surface of the tungsten carbide particle seems very even. The erosion of the material takes place mainly via formation of cracks in radial as well as parallel to the surface or following the crystallographic orientation of the carbide particle. As a result, pieces of carbide will be removed.

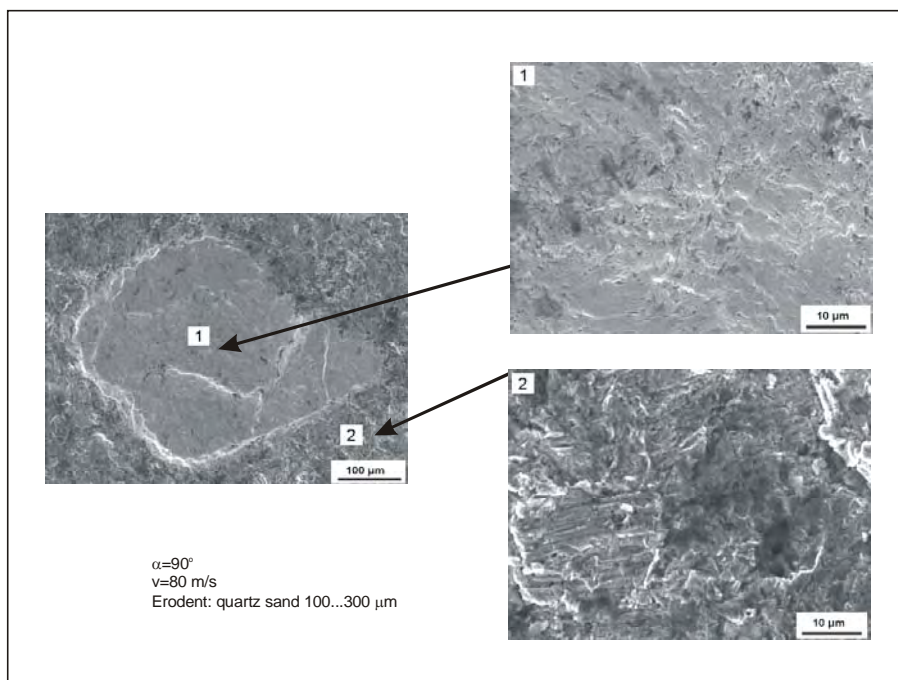


Figure 4.7 SEM images of the eroded surfaces of the PM MMC material (Cr steel+VC) + WC.

The wear surfaces of the self-fluxing FSF (NiCrSiB) + (WC-Co) coating was investigated after the erosion test in identical conditions: quartz sand with the mean particle size of 100...300 μm and

velocity of 80 m/s. The SEM images of the surface subjected to erosion at 30° and 90° are given in Figs 4.8 and 4.9, respectively.

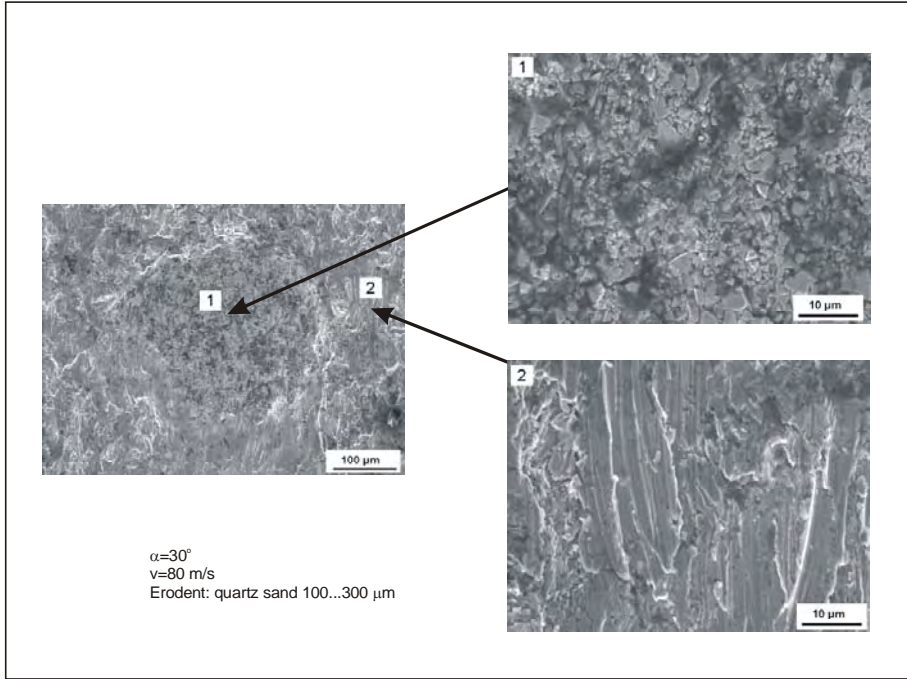


Figure 4.8 SEM images of the eroded surfaces of the self-fluxing FSF (NiCrSiB) + (WC-Co) coating

As it follows from Fig. 4.8, at low impact angles the mechanism of microcutting becomes even more evident than in the case of the MMC material with the Cr steel matrix phase. As the NiCrSiB-based alloy has lower hardness, the erodent particles are capable of producing grooves reaching the border area of the reinforcing phase. Erodent particles with smaller size are able to cause erosion of the binder phase of the hardmetal particle. After removal of the Co phase, the WC grains will separate also. Larger particles of the erodent the size of which is comparable to the size of the reinforcing phase – WC-Co hardmetal particles cause a direct fracture of hardmetal particles after multiple collisions.

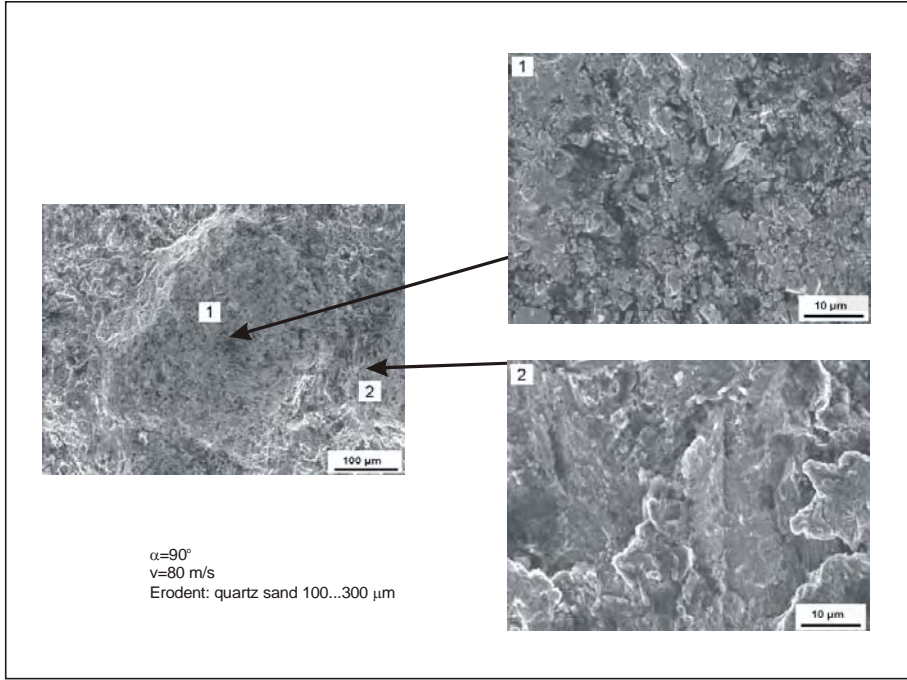


Figure 4.9 SEM images of the eroded surfaces of the self-fluxing FSF coating (NiCrSiB) + (WC-Co).

To investigate the transition of wear mechanisms, in the tests the particle size of the erodent was varied. In Fig. 4.10, an eroded surface of the (Cr steel+VC)+WC PM MMC material is presented after testing with quartz sand dust at 60°. The particles of the erodent with a size of 10...30 µm are too small to cause clearly visible wear traces, indents and grooves.

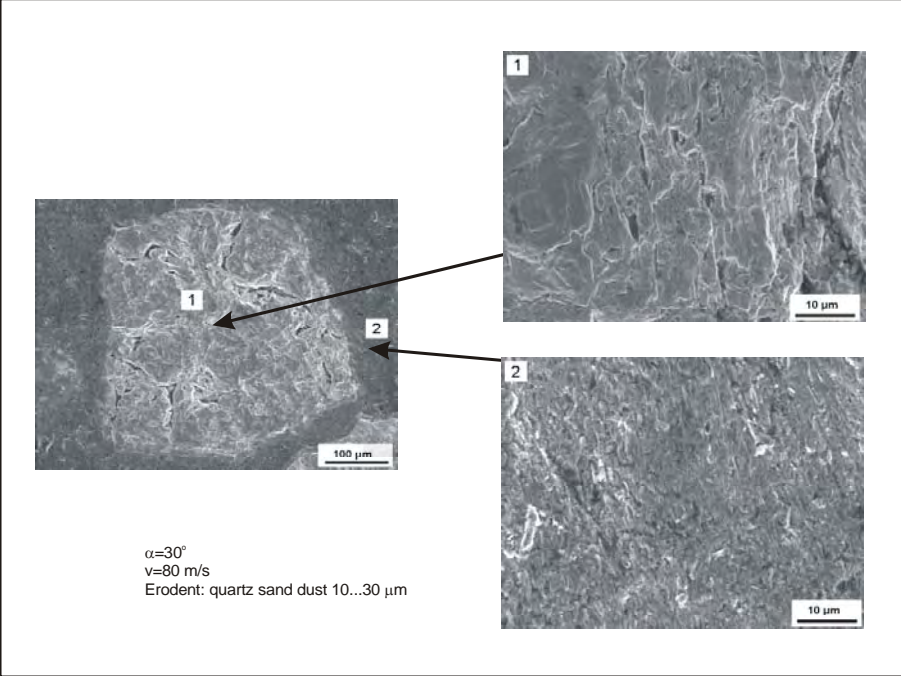


Figure 4.10 SEM images of the eroded surfaces of the PM MMC material (Cr steel+VC)+WC.

Apparently, the erosion of the matrix will take place by the mechanism of microcutting after which the particles of the reinforcing phase become loose and separate eventually. The surface and edges of a hard carbide particle stay intact and relatively even, no direct fracture can be observed.

The erosion wear of the same MMC material subjected to impacts at 60° by the erodent particles one order larger in size will take place according to the combined mechanism of erosion. The plastic deformation of the Cr steel matrix can be observed (see Fig. 4.11).

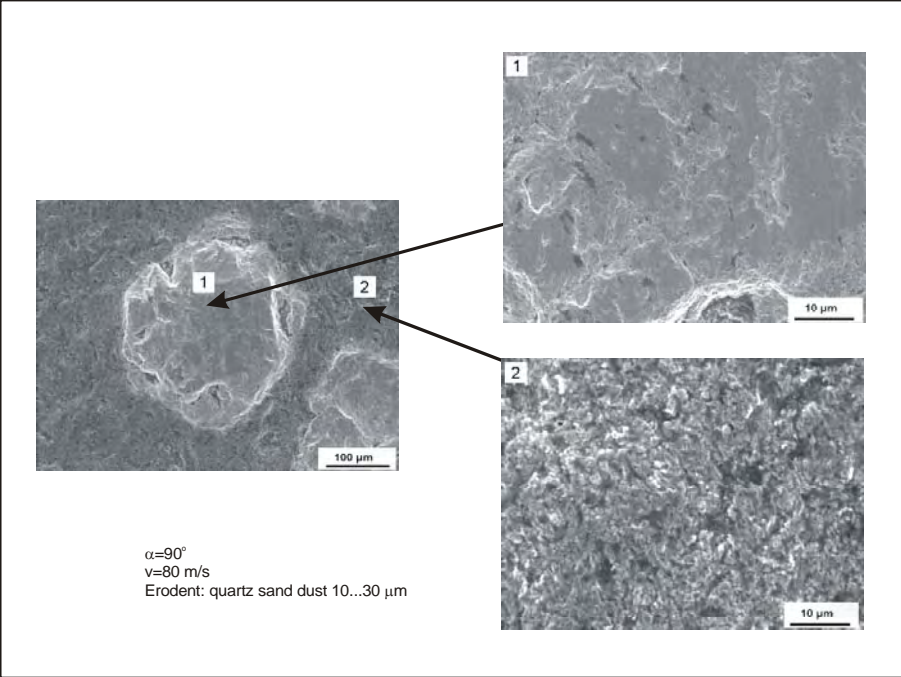


Figure 4.11 SEM images of the eroded surfaces of the PM MMC material (Cr steel+VC)+WC.

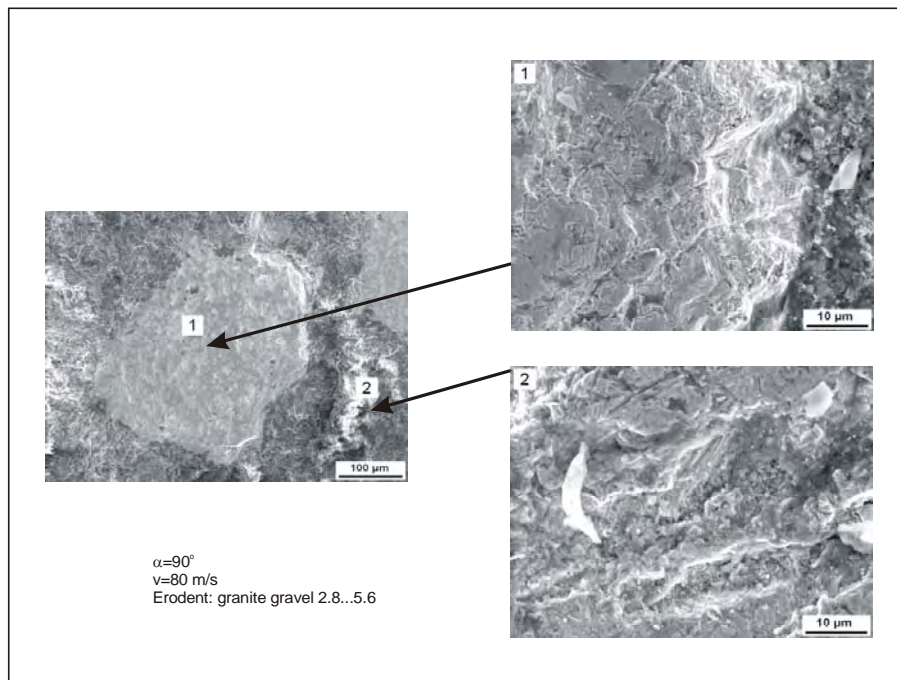


Figure 4.12 SEM images of the eroded surfaces of the PM MMC material (Cr steel+VC)+WC.

Also, the carbide phase reveals marks of direct fracture. The edges of the carbide particle are not as even and smooth as in the conditions of dust erosion. The energy of impinging particles is mostly insufficient to cause direct fracture of carbide in those conditions of wear; it requires multiple impacts to fracture the carbides and to separate the small carbide pieces. As the hard phase particles will be excrescent from the material surface, they become eventually more vulnerable to the impacts of the erodent particles.

The SEM images of the eroded surface of the (Cr steel+VC)+WC MMC material subjected to the impact wear are presented in Fig. 4.12. Granite particles with average hardness HV0.1 1050...1100 and mean particle size of 2.8...5.6 mm cause a noticeable wear loss after a while. As it follows from Fig. 4.12, the ploughing and the cutting mechanisms in a smaller scale prevail in the degradation of the matrix. The direct fracture of carbide particles was not noticed at first due to the size (about 30...50 times larger than WC particles) of the abrasive.

This can partly be explained by the properties of the erodent: first, due to the low toughness of granites and secondly most of the energy will be consumed during the impact for crack propagation and erodent particles crushing. In several cases, the edges of the carbides were broken; smaller splinters and fragments will separate due to direct fracture. The mechanism includes the penetration of the eroding particles into the surface forming craters (Fig. 4.12). Wear at this type of high-energy impact is caused by low-cycle fatigue, occurring at repeated dynamic loading. As it was demonstrated, high wear resistance at impact wear guarantees the using of Co-rich WC-Co hardmetals (relative wear resistance about 5.5 times higher than Hardox 400).

5 CALCULATION OF EROSION WEAR USING PARAMETERS DETERMINED BY DIFFERENT INDENTATION METHODS

5.1 Calculation principles

The plastic contact is dominating by the metal-matrix of materials and coatings and the model of plastic deformation is applicable. With the hardmetal type coatings, where carbide content exceeds 50%, brittle fracture of carbide is dominating. With composite metal-matrix materials, both models must be taken into consideration: by the relatively soft metal matrix – the model of plastic deformation (Eq. (1.2)), by the hard-phase – the models of plastic deformation and brittle fracture (Eq. (5.1)).

The wear rate of hardness consists of a portion of brittle fracture with weight p and a portion of the plastic deformation with weight $1-p$.

$$I^{B\&P}(H_i) = \{I^B(H_i) \cdot p(H_i) + I^P(H_i) \cdot [1 - p(H_i)]\} \cdot f(H_i) \cdot \frac{\Delta H}{n}, \quad (5.1)$$

$$\text{where } f(H_i) = \frac{m}{H_0} \left(\frac{H_i}{H_0} \right)^{m-1} \cdot \exp \left\{ - \left(\frac{H_i}{H_0} \right)^m \right\} \quad (5.2)$$

is the probability density function of the Weibull distribution (see Eq. (2.3)).

In the calculations, the following materials served as examples:

- Cr steel based PM produced metal-matrix composite (MMC) material, containing about 20 vol% of VC micrometrical particles and about 20 vol% of WC reinforcement with particle size about 200 μm ,
- thermal spray-fused self-fluxing NiCrSiB alloy based MMC coating, containing about 20 vol% (WC-Co) hardmetal reinforcement with particle size about 100...300 μm .

Table 5.1 Initial data for calculation of erosion wear of composite metal-matrix structures

Components	ρ_1 kg/m ³	H_1 (HV) GPa	E_1 GPa	μ_1	K_{1c} MPa·m ^{1/2}	Reduced modulus of elasticity E' GPa	Contact hardness H_c , GPa		K_{1c}^4/H_1^3 N
							$\alpha = 30^\circ$	$\alpha = 90^\circ$	
Commercial NiCrSiB alloy coating	8900	4.8	217	0.21	-	-	-	-	-
Commercial tool steel WR-6	7400	3.8	220	0.28	-	-	-	-	-
<u>Matrices</u>									
- NiCrSiB alloy matrix	8900	5.6	175	0.21	75	61.5	2.8	2.4	180
- Cr steel matrix	7400	6.8	220	0.28	15	66.8	1.8	2.1	161
<u>Hard phases</u>									
- WC hard phase	15800	24.5	680	0.22	5-11	82.0	3.5	3.0	$8.7 \cdot 10^{-5}$
- WC-15Co hard phase	14500	14.0	560	0.23	12	80.1	3.4	2.96	$7.6 \cdot 10^{-3}$
Quartz sand $R_2 = 0.05\text{-}0.15$ mm	2200	11.5	E_2 90	μ_2 0.17	0.7	-	-	-	15.8

For the six mean values of hardness intervals calculated in Chapter 4, the plastic penetration depth of indentation h_p (Eq. (1.9)), the corresponding radii of indentation r_n

$$r_n = R_2 \left[\left(h_p / R_2 \right)_i - \left(h_p / R_2 \right)_i^2 \right], \quad (5.3)$$

the normal force F_n of crack initiation

$$F_n = H_n \cdot \pi \cdot r_n^2 \quad (5.4)$$

and the probability of brittle fracture p according to Eq. (2.3) were found (see Annex A, Tables A1–A3 for MMC material and A7–A8 for MMC coating).

The values of parameters τ_o/e_s were determined (Table 5.2) with the help of Fig. 1.3 using the mean hardness values of the constituents (correspondingly 4540 and 13 240 MPa for MMC material and 3000 and 6600 for MMC coating). For the metal matrix and the hard phase the values of τ_o/e_s 0.1 and 0.06 were chosen for matrices and 0.5 and 0.15 for hard phase, respectively and used in the calculations according to Eq. (1.1).

Table 5.2 Values of τ_o/e_s

Type of material	Metal matrix	Hard phase
(Cr steel -VC)+WC	0.1-0.13	0.3-1.0
NiCrSiB+(WC-Co)	0.05-0.1	0.1-0.3

5.2 Calculation of erosion rate of MMC material

Based on the hardness distribution of HU1 and parameters H_0 and m obtained from the Weibull distribution function (Eq. 1.5), applying the calculus algorithm given above (Eqs. (1.1) and (1.2)) and taking into account the probability of brittle fracture, the erosion rates were calculated for each hardness interval. Calculation results are given in Annex A (Tables A5–A8)

Table 5.3 demonstrates the calculated values of important parameters such as the diagonal of the cavity created by the impact of erodent particle and the calculated erosion rate mg/kg at impact angles 30° and 90°. The hardness values of universal hardness HU1 taken into consideration varied from 4073 to 12 336 MPa. The values of erosion rates from plastic and brittle wear are given in Table A5 (I_g^P and I_g^B respectively). It can be seen (Fig. 5.1), that the calculus algorithm strongly overestimates the wear caused by brittle fracture in the range of mean values of hardness HU1 7517-11 650 MPa.

Table 5.3 Theoretical dimensions of the cavities and calculated erosion rates of MMC material based on universal hardness HU1 (erodent – quartz sand, $R_2=0.1$ mm, $v=50$ m/s)

Mean hardness HU1 of interval, MPa	Indent diagonal μm	Impact angle $\alpha=30^\circ$		Impact angle $\alpha=90^\circ$	
		$r_n, \mu\text{m}$	$I_g, \text{mg/kg}$	$r_n, \mu\text{m}$	$I_g, \text{mg/kg}$
4762	62.5	16.5	11.5	23.4	12.1
6140	55.0	15.3	9.58	21.9	10.6
7517	49.5	14.4	271	20.8	804
8895	46.5	13.3	137	19.7	429
10 273	42.5	11.6	33.2	18.7	151
11 650	40.0	6.79	0.9	17.6	33.2
Total erosion rate			463		1440

Table 5.4 demonstrates the calculated values of indentation diagonals of the cavities and the calculated erosion rate on the basis of the HV0.1 measurements. The hardness values of microhardness HV0.1 taken into consideration varied from 3080 to 20 490 MPa. The relative weights of metal matrix and hard phase in structure (correspondingly 0.74 and 0.26), following from the experimental cumulative hardness distribution function, were applied. For hardness ranges with mean hardness more than 10340 MPa (included), the model of brittle fracture was applied by dividing the hardness range 8890...20 490 into four hardness ranges.

Table 5.4 Theoretical dimensions of the cavities and calculated erosion rates of MMC material based on microhardness HV0.1 (erodent – quartz sand, $R_2=0.1$ mm, $v=50$ m/s)

Mean hardness HV0.1 of interval, MPa	Indent diagonal μm	Impact angle $\alpha=30^\circ$		Impact angle $\alpha=90^\circ$	
		$r_n, \mu\text{m}$	$I_g, \text{mg/kg}$	$r_n, \mu\text{m}$	$I_g, \text{mg/kg}$
4540	20.2	16.7	39.3	23.6	40.9
7440	15.8	14.0	0.89	20.7	10.6
10340	13.4	11.4	9.33	18.7	26.5
13240	11.8	0	0	15.7	107.0
16 140	10.7	0	0	0	0
19 040	9.8	0	0	0	0
Total erosion rate			49.6		176

In the next calculation stage the hardness values of microhardness HV0.1 on the basis of the relative weights of metal matrix and hard phase in the structure (correspondingly 0.78 and 0.22, following from the experimental cumulative hardness distribution function), were taken into consideration. In the hardness range from 8890-20 490 new parameters of hardness distribution H_0 and m were determined and the wear rates for these six hardness ranges were calculated. The best coincidence of experimental and theoretical hardness distributions was achieved at $H_0=17.9$ and $m=7.9$.

The values of erosion rates from plastic and brittle wear are given in Table A7 Annex A (I_g^P and I_g^B respectively). Table 5.5 demonstrates the calculated values of indentation diagonals of the cavities and the calculated erosion rate on the basis of the HV0.1 measurements.

Table 5.5 Theoretical dimensions of the cavities and calculated erosion rates of MMC material based on microhardness HV0.1 at new hardness distribution (erodent – quartz sand $R_2=0.1$ mm, $v=50$ m/s)

Mean hardness HV0.1 of interval, MPa	Indent diagonal μm	Impact angle $\alpha=30^\circ$		Impact angle $\alpha=90^\circ$	
		$r_n, \mu\text{m}$	$I_g, \text{mg/kg}$	$r_n, \mu\text{m}$	$I_g, \text{mg/kg}$
4540	20.2	16.7	39.3	23.6	40.9
7440	15.8	14.0	0.9	20.7	1.1
9860	13.6	12.2	5.6	19.0	13.3
11 800	12.4	0.37	0.4	17.4	39.4
13 740	11.5	0	0	14.9	85.4
15 690	10.8	0	0	0	0
17 630	10.2	0	0	0	0
19 570	9.6	0	0	0	0
Total erosion rate			46.2		180.0

In nanohardness scale the hardness taken into consideration varied from 1380 to 10 010 MPa for matrix phase only. Although only the hardness distribution of the matrix phase reinforced with VC particles is taken into account in the erosion wear calculations, the predicted wear rate coincides well with experimental erosion wear test results. Table 5.6 demonstrates the calculated value of indentation diagonals of the cavities and the calculated erosion rate on the basis of the H_{nano} measurements.

Table 5.6 Theoretical dimensions of the cavities and calculated erosion rates of MMC material based on nanohardness H_{nano} (erodent - quartz sand, $R_2=0.1$ mm, $v=50$ m/s)

Mean hardness H_{nano} of interval, MPa	Indent diagonal μm	Impact angle $\alpha=30^\circ$		Impact angle $\alpha=90^\circ$	
		$r_n, \mu\text{m}$	$I_g, \text{mg/kg}$	$r_n, \mu\text{m}$	$I_g, \text{mg/kg}$
2100	0.55	20.3	20.4	28.6	18.3
3540		17.8	11.6	25.2	11.4
4980		16.3	4.88	23.1	5.17
6420		15.1	14.6	21.6	26.3
7860		13.9	4.67	20.4	10.8
9300		12.2	1.19	19.3	3.78
Total erosion rate			57.3		75.8

The calculated and the experimental results of the wear rates of MMC material with multimodal reinforcement and a relatively high content and wide range of reinforcing particle size showed a major difference. The results of experimental and calculated wear rates are given in Figure 5.1. The discrepancy between the calculated wear rates obtained by universal hardness and experimental wear rates is caused at first by the big difference in indent parameters and cavities formed by the abrasive particles (indent diagonal 40...62.5 μm , erosion cavities 13...33 μm .). If the hardness parameters determined with HV0.1 were used, the difference between experimental and calculated results was minimal at oblique impact (Fig. 5.2). The predicted erosion rate at normal impact exceeds the experimental erosion rate about two times. It can be explained by the following:

- The size of the WC reinforcing particles features, which determines the range of hardness distribution, does not correlate with input parameters for erosion wear calculation model. If the size of the indents produced by the selected hardness measurement method is in the same order of size as the cavities produced by the erodent particle, the hardness distribution can be used for wear calculation.
- The nonconformity between experimental and calculated results may also indicate that the probability of the brittle fracture is overestimated and fracture toughness parameters characterizing the brittle fracture mechanism should be determined with better accuracy.

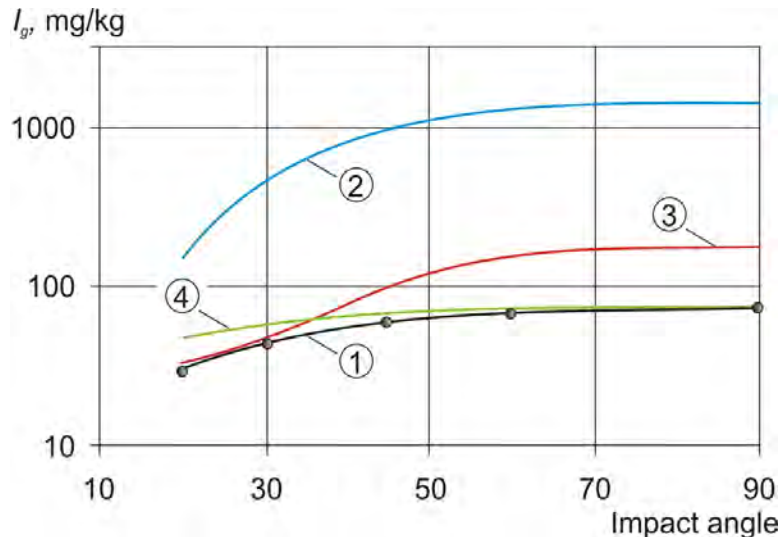


Fig. 5.1 Dependence of experimental (1) and calculated wear rates on the impact angle using HU1 (2), HV0.1 (3) and H_{nano} (4) hardness of MMC material

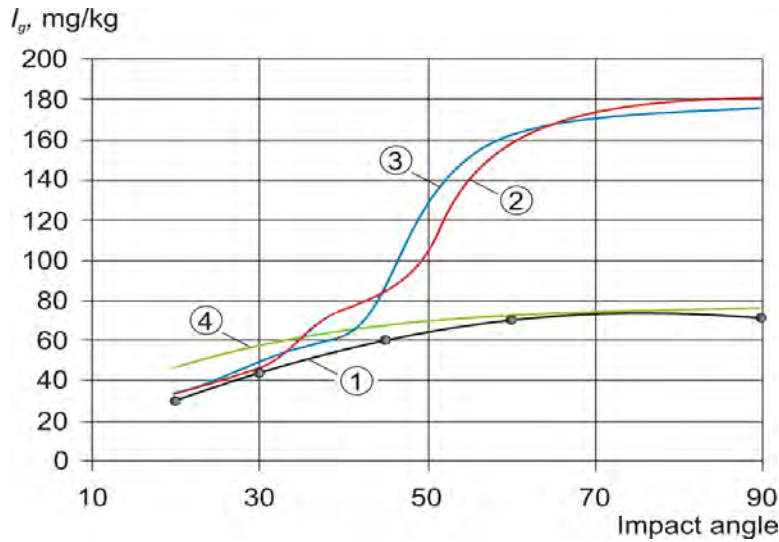


Fig. 5.2 Dependence of wear rates of MMC material on the impact angle: experimental (1) and calculated using HV0.1 based on four hardness intervals (2), using HV0.1 based on six hardness intervals (3) and using H_{nano} (4) hardness

5.3 Calculation of erosion rate of MMC coating

Based on the hardness distribution of HU1 and parameters H_0 and m obtained from the Weibull distribution function (Eq. (1.5)) the calculation of erosion rate for MMC coating material NiCrSiB-20 vol % (WC-Co) was carried out similarly as it was done for MMC material. Table 5.7 demonstrates the calculated parameter of the cavities (r_n) and the calculated erosion rate on the basis of the HU1 measurements. The values of plastic and brittle wear (I_g^P and I_g^B) are given in Table A11, Annex A.

Table 5.7 Theoretical dimensions of the cavities and calculated erosion rates of MMC coating based on universal hardness HU1 (erodent – quartz sand, $R_2=0.1$ mm, $v=80$ m/s)

Mean hardness HU1 of interval, MPa	Indent diagonal μm	Impact angle $\alpha=30^\circ$		Impact angle $\alpha=90^\circ$	
		$r_n, \mu\text{m}$	$I_g, \text{mg/kg}$	$r_n, \mu\text{m}$	$I_g, \text{mg/kg}$
1177	127.0	29.5	176	41.3	116
2392	88.0	24.8	72	34.8	55
3606	72.0	22.4	29	31.5	24
4820	62.0	20.8	11	29.4	10
6034	55.0	19.7	29	27.8	50
7248	50.5	18.7	11	26.5	19
Total erosion rate			328	274	

Experimental results of the wear rates of the Ni-based matrix composite coating by the observation abrasive observed– quartz sand ($H_m < H_a$) with particles velocity 80 m/s at impact angles from 30° to 75° had a very good coincidence (Fig. 5.2).

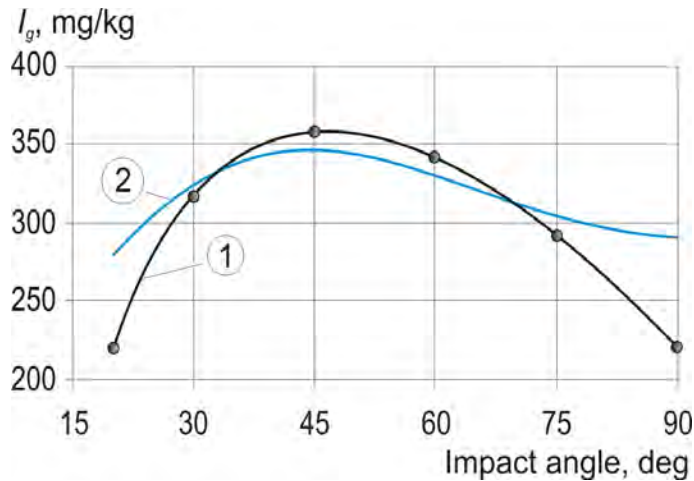


Fig. 5.3 Dependence of experimental (1) and calculated (2) wear rates on the impact angle of MMC coating,

The difference in the results at small impact angles (the calculated values of wear rate are higher) indicates the necessity to correlate the shear energy density; the difference at straight impact may be explained with the accuracy of K_{1c} determination.

Based on the results obtained by different hardness measurement scales, the following conclusions can be drawn:

1. The model of plastic deformation is applicable if the ratio $H_a/H_m > 1.6$, as the erodent is able to generate plastic deformation of the material, producing grooves and craters. In case of quartz sand as erodent (with HV 1100...1200), the model can be used if the hardness of the material is below 750 HV (Fig. 5.4, area A). This was also the hardness of the matrix phase of the studied MMC material.
2. As the ratio of the hardness of the abrasive and material the $H_a/H_m < 1.6$, the brittle fracture of hard phase becomes dominant in erosion wear (Fig. 5.4, area B). Nevertheless, this is limited by the hardness ratio of $H_a/H_m < 0.5$.
3. The constraints to the applicability of a brittle wear model are set also by the ratio between fracture toughness values of the material and abrasive. If the ratio $K_{1c}(\text{material})/K_{1c}(\text{abrasive}) > 15...20$, the fracture probability p equals zero and the fracture of the reinforcing phase requires multiple impacts – the mechanism of erosion could be described as surface fatigue mechanism (Fig. 5.4, area C).

Figure 5.4 illustrates the proposed limits of different erosion models.

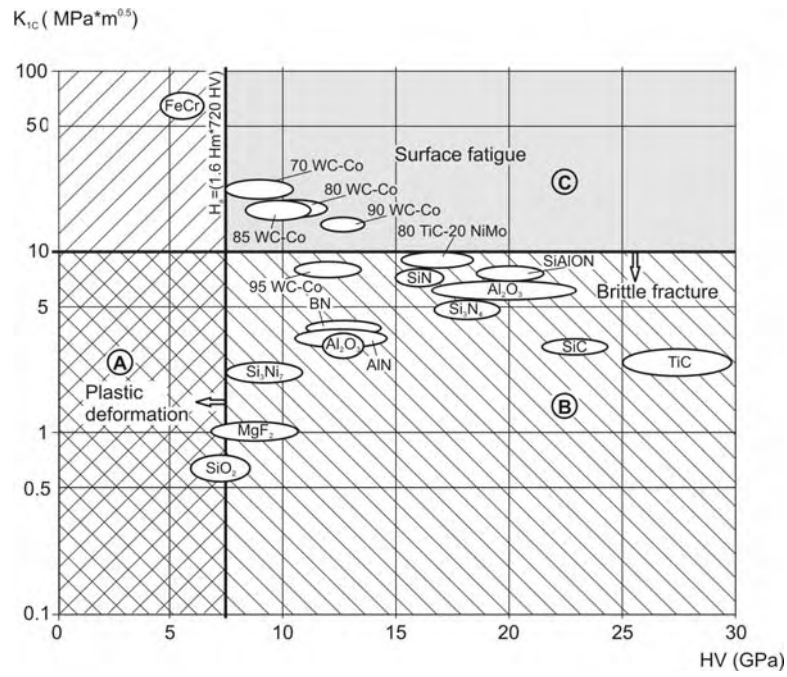


Fig.5.3 Realizing models and existing limits of erosion wear: area A – plastic deformation, area B – brittle fracture and area C – surface fatigue.

CONCLUSIONS

1. Tribological materials and coatings are typical of heterogeneous structure, ie. hard particles in a relatively soft matrix, and typical representatives of erosion resistant materials. Such materials are metal-matrix composite (MMC) materials and coatings with particulate hard reinforcements. Most of the information available on the tribological properties of these materials and coatings has been derived from the laboratory tests rather than engineering applications. Attempts have been made to correlate the erosion rate of homogeneous materials with experimental parameters and mathematical models by Beckmann, Kleis and Gotzmann. In these models, shear energy density, hardness and fracture toughness emerge as the main materials parameters that control erosion.

The main objectives of the study were:

- experimental determination of the important mechanical parameters of MMC materials and coatings used in the mathematical model of erosive wear, and an analysis of erosion resistance and wear mechanisms of MMC materials and coatings with multimodal reinforcements;
 - development of a mathematical model based on the combined model of plastic deformation and brittle fracture, using hardness and toughness parameters obtained by indentation methods.
2. The following metal-matrix composite materials and coatings with multimodal reinforcements were studied:
 - powder metallurgically (PM) produced Cr steel based metal-matrix, consisting of sub-micron size VC particles and coarse carbides of WC, TiC or NbC as main reinforcement;
 - flame-spray-fused (FSF) coatings based on self-fluxing NiCrSiB alloy matrix, dispersion-strengthened with carbides, borides and silicates of Cr and Ni and (WC-Co) hardmetal particles as main reinforcement.

The variation of the volume fraction of the reinforcement phase allows creation of materials with unique properties for a variety of tribological applications and a study of the relations between properties and wear behaviour of those materials.

3. For the characterization of hardness-toughness properties of the PM MMC materials and FSF MMC coatings with multimodal reinforcements, the indentation methods were used:
 - hardness measurements in different scales (macro-, micro- and nanoscale) for the evaluation of hardness distribution of the MMC structures were carried out. It was demonstrated that the hardness range and the individual hardness values varied on a large scale.

The method of continuous indentation or the depth sensing hardness test, also referred to as instrumented or universal hardness HU, is preferred to characterize erosive wear behaviour of MMC materials and coatings.
 - to determine fracture toughness as the main parameter besides hardness, describing the brittle fracture and fracture probability of the hard phase during the erosion process, the indentation method may be used.
 - the indentation method and parameters selection are based on the presumption that the indents produced by the hardness measurement and during the process of erosive wear

when the abrading particle is bulging into material surface, must have similar geometry, e.g. similar depth and/or diameter.

4. The wear performance of MMC materials and coatings with heterogeneous structure was tested under different conditions of solid particle erosion with erodents of particles size from some tens μm up to 3...5 mm. The influence of reinforcement (WC, TiC, NbC) in steel-matrix based MMC materials and WC-Co in the self-fluxing alloy based matrix on the erosion rate and relative erosive resistance was clarified.

The tested MMC materials revealed at low velocities (from 20...50 m/s) and at low impact angles compared to the steels a higher erosion resistance; the relative erosion resistance of material reinforced with TiC was about 2.5 times higher than that of AISI316. At higher velocities and with a coarser abrasive, the advantages of material B reinforced with WC were demonstrated – relative wear resistance of this material with abrasive 2.8...5.6 mm was up to four times higher compared with Hardox 400 steel. The peculiarities of the wear mechanism of MMC materials with multimodal reinforcement were determined. The wear of the metal-matrix results from plastic deformation and microcutting of the dispersion strengthened metal matrix, forming grooves and craters. With tungsten carbide, relatively resistant to the impact of erodent particles of studied size and velocities, a fracture occurs due to the removing of matrix metal around the carbides, debonding and separating them. The abrasive particle, with a size comparable to that of the carbides, causes a direct fracture of the carbide particle and separation of smaller splinters from them. The relative erosion resistance of the MMC coating based on a self-fluxing alloy and WC-Co reinforcement at low impact angle was about two times higher than that of steel C=0.45%. Wear mechanisms of NiCrSiB alloy based metal matrix and WC-Co reinforcement are similar to those of MMC materials. At high impact angles, the low-cyclic fatigue of the matrix and WC-Co hardmetal is dominating.

5. The concept of plastic deformation and brittle fracture and the proposed combined model of erosion can be applied for the calculation of the wear of materials with a composite structure. With a relatively soft metal matrix, the energetic theory of wear using the mean hardness and dimensionless specific energy parameter τ_0/e_s is applicable. In the wear calculations of the hard phase, the models of plastic deformation and brittle fracture using hardness distribution and fracture probability, must be taken into consideration.

The calculated and the experimental results of the wear rates of the MMC material with multimodal reinforcement (reinforcing phase in a wide range of particle size) showed a major difference. This difference indicates that fracture toughness parameters characterizing the brittle fracture mechanism should be determined with higher accuracy.

The calculated and experimental results of the wear rates of the Ni-based matrix composite coating with a relatively low hardness ($H_m < H_a$) had a very good coincidence.

6. On the basis of the studies of erosion wear mechanisms and the results of wear calculation, further research to characterize and model erosion resistant MMC materials and coatings will be focused on the following:
 - determination of the shear strength and shear energy density τ_0/e_s of dispersion-strengthened metal-matrices of MMC materials;
 - determination of the main characteristics of MMC materials such as hardness-toughness properties at dynamic loading as well as contact fatigue and residual stresses of MMC materials and their constituents – metal-matrix and reinforcements using indentation methods;
 - modification of the mathematical model of erosion wear for composite structures, involving the model parameters of the target material (dynamic hardness) as well as parameters of the erodent (fracture toughness at high energy impact and particle shape parameter at oblique impact, etc.);

- development of standardized measurement procedures and calculation methods to improve the accuracy in determination of the fracture toughness K_{Ic} by indentation methods.

References

1. Holmberg, K., Matthews, A., Coatings Tribology Properties, Techniques and Applications in Surface Engineering. Elsevier, 1994. 441 p.
2. Kallas, P. Abrasive Erosion of Powder Materials. PhD Thesis, Tallinn, 1996. 24 p.
3. Reshetnyak, H., Kübarsepp, J., Mechanical properties of hard metals and their erosive wear resistance, *Wear*, Vol. 177 (2), 1994, pp. 185-193.
4. Hussainova, I., Kübarsepp, J., Pirso, J., Mechanical properties and features of erosion of cermets, *Wear*, Vol. 250, 2001, pp. 818-825.
5. Hussainova, I., Effect of microstructure on the erosive wear of titanium carbide-based cermets, *Wear*, Vol. 255, 2003, pp. 121-128.
6. Kleis, J., Pappel, T., Proc. of the 6th Nordic Symposium on Tribology, NORDTRIB 95, Uppsala, Sweden, Vol I, 1994, pp. 215-223.
7. Kulu, P., The abrasive erosion resistance of powder coatings, *J. Tribologia: Finnish J. Tribology*, Vol 8 (4), 1989, pp. 12-25.
8. Kulu, P., Halling, J. Recycled hard metal-base wear-resistant composite coatings *J. Thermal Spray Technology*, 7, Vol. 2, 1998, pp. 173-178.
9. Kulu, P., Zimakov, S., Wear resistance of thermal sprayed coatings on the base of recycled hardmetal, *J. of Surface and Coating Technology*, 130, 2000, pp. 46-51.
10. Wellinger, K., Uetz, H., Gleitverschleiss, Spülverschleiss, Stahlverschleiss unter der Wirkung von körnigen Stoffen, *VDI – Forschungsheft 449*, Ausgabe 13, Band 21, 1955.
11. Finnie, I. G., Wear Control Technology: Source Book American Society for Metals, 1978, pp. 220-236.
12. Beckmann, G., Kleis, I., Abtragverschleiß von Metallen, VEB Deutscher Verlag für Grundstoffindustrie, Leipzig 1983, p. 184.
13. Gotzmann, J., Modellierung des Strahlverschleißes an keramischen Werkstoffen, *Schmierungstechnik, Fachzeitschrift für Tribotechnik*, VEB Verlag Technik Berlin, 20, 1989, 11, p. 324-329.
14. Weiler, W., Hardness testing – a new method for economical and physically meaningful micro-hardness testing, *Br. J. of Nondestructive Testing*, 31, 1989, pp. 253-258.
15. Pawlowski, L. The Science and Engineering of Thermal Spray Coatings. John Wiley & Sons, 1995 275 p.
16. ISO/EN 14577 - 1, 2 & 3: 1999, Metallic materials – Instrumented indentation test for hardness and other material properties.
17. Giannakopoulos, A. E., Suresh, S., Determination of elastoplastic properties by instrumented sharp indentation, *Scripta Materialia*, 40 (10), 1999, pp. 1191-1198.
18. Factor, M., Roman, I., Vickers microindentation of WC-12%Co thermal spray coating. Part 1: statistical analysis of microhardness data, *Surface and Coatings Technology*, 132, 2000, pp. 181-193.
19. Valente, T., Statistical evaluation of Vicker's indentation test results for thermally sprayed materials, *Surface and Coatings Technology*, Vol. 90 (1-2), 1997, pp. 14-20.
20. Lin, C. K., Berndt, C. C., Proceedings of the National Thermal Spray Conference, ASM, 1993, pp. 561-564.
21. Oliver, W.C., Pharr, G. M., An improved technique for determining hardness and elastic modulus using load and displacement sensing indentation experiments, *J. of Material Research* 7, 1992, pp.1564-1583.

22. Greenwood, J.A., Williamson, J. B., Contact of nominally flat surfaces. *Proc. Roy. Soc Londo, Cer. A*, 295, 1966, pp. 300-319.
23. Kleis, I., Probleme der Bestimmung des Strahlverschleißes bei Metallen, *Wear*, 13, (3), 1969, pp. 199-215.
24. Zhang, S., Sun, D., Fu, Y, Du, H., Toughness measurement of thin films: a critical review, *J. Surface and Coatings Technology*, 198, 2005, pp. 74-84.
25. Wayne, S. F., Sampath, S., Structure/property relationships in sintered and thermally sprayed WC-Co, *J. Thermal Spray Technology*, 1 (4), 1992, pp. 307-315.
26. Palmqvist, S., *Archiv für das Eisenhüttenwesen*, Vol. 33, 1962, pp. 629-633.
27. Marshall, D. B., Lawn, B. R., Indentation of Brittle Materials, *Microindentation Techniques in Materials Science and Engineering*, ASTM STP 889 (Eds. P. J Blau and B. R. Lawn), Philadelphia, pp. 26-46.
28. Ponton, C. B., Rawlings, R. D., Vickers indentation fracture toughness, Part 1: Test review of literature and formulation of standardised indentation toughness equations. *J. Material Science and Technology*, Vol. 5, 1989, pp. 865-872.
29. Niihara, K., Morena, R., Hasselman, D.P.H., Evaluation of K_{Ic} of brittle solids by the indentation method with low crack-to-indent ratios, *Journal of Material Science Letters*, 1, 1982, pp. 13-16.
30. Niihara, K., A fracture mechanics analysis of indentation induced Palmqvist cracks in ceramics, *Journal of Material Science Letters*, 2, 1983, pp. 221-230.
31. Shetty, D. K., Wright, I. G., Mincer, P. N., Clauer, A. H., Indentation fracture of WC-Co cermets, *Journal of Material Science* 20, 1985, pp. 1873-1882.
32. Laugier M. T., New formula for indentation toughness in ceramics, *Journal of Material Science Letters*, 6, 1987, pp. 355-256.
33. Anstis, G. R., Chantikul, P., Lawn, B. R, Marshall, D. B., A critical evaluation of indentation techniques for measuring fracture toughness: I Direct crack measurements, *J. Am. Ceramic. Soc.*, 64 (5), 1981, pp. 533-538.
34. Tabor, D., *The Hardness of Metals*, Oxford Univ. Press, 1951.
35. GOST 23.201-78, Products wear resistance assurance. Gas abrasive wear testing of materials and coatings with centrifugal accelerator, Moscow: Publishing House of Standards, 1987 (in Russian).
36. López Cantera, E., Mellor, B. G., Fracture toughness and crack morphologies in eroded WC-Co-Cr thermally sprayed coatings, *Materials Letters*, 37, 1998, pp. 201-210.
37. Malzbender, J., de With, G., The use of indentation loading curve to detect fracture of coatings, *J. Surface and Coatings Technology*, 137, 2001, pp. 72-76.

KOKKUVÕTE

PULBERKOMPOSIITMATERJALIDE JA -PINNETE OMADUSED JA EROSIONKULUMISE MODELLEERIMINE

Töös on uuritud metall-maatrikskomposiitmaterjalide (MMKM) ja -pinnete abrasiiverosioonkulumise ning mikromehaaniliste omaduste vahelisi seoseid.

Silmas pidades selliste nn. topeltarmeeritud ehk multimodaalsete materjalide üksikute struktuuriosade kõvadus- ja sitkusomadusi, on edasi arendatud erosioonkulumise teooriat, mis tugineb kulumise prognoosimisel kõvaduse jaotusfunktsiooni parameetrite kasutamisel. Katsetulemuste ja arvutusmudelil lähtuvate tulemuste kõrvutamisel on leitud sobivaim meetod MMK-materjalide erosioonkulumise prognoosimiseks.

Läbi on viidud laboratoorsed katsed eksperimentaalsete MMK-materjalide ja -pinnetega, uurimaks nende vastupanu kulumisele erinevates tingimustes (varieerides abrasiivi suurust ja kiirust).

Näidati, et kulumise prognoosimisel ei ole õigustatud kõvaduse ja purunemissitkuse keskväärtuste kasutamine, mis on nii teaduskirjanduses kui ka tööstuses levinud praktika. Tingituna MMK materjalide heterogeensest struktuurist on otstarbekam kasutada kõvaduse (ja sitkuse) jaotust, mida sobib kõige paremini kirjeldama Weibulli jaotus.

Viidi läbi kulumispindade struktuuriuuringud ning selgitati välja uuritavate materjalide kulumismehhanismide erinevused.

Elulookirjeldus (CV)

- | | |
|--|---|
| 1. Eesnimi | Renno |
| 2. Perekonnanimi | Veinthal |
| 3. Töökoht | Tallinna Tehnikaülikool, materjalitehnika instituut |
| 4. Ametikoht | teadur |
| 5. Sünniaeg | 24.07.1976 |
| 6. Haridus | 2001- 2005 TTÜ doktoriõpe, tootmistehnika õppesuund;
1999-2001 TTÜ tootmistehnika õppesuund, tehnikamagister;
1994-1999 TTÜ tootmis- ja transporditehnika õppesuund, insener
(viieaastane kraadieelõpe);
1986-1994 Tallinna Kadrioru Keskkool |
| 7. Teenistuskäik | 01.09.1999 teadur, Tallinna Tehnikaülikool
16.09.1996 insener, Tallinna Tehnikaülikool |
| 8. Teaduskraad | tehnikamagister |
| 9. Teaduskraadi välja
andnud asutus, aasta | Tallinna Tehnikaülikool, 2001 |
| 10. Tunnustused | Eesti Teaduste Akadeemia 1999. a. lõputööde konkursi preemia
diplomitöö "Materjalide ja toodete mittepurustav kontroll" eest |
| 11. Teadusorganisatsiooniline
ja –administratiivne
tegevus | 2004-praeguseni Majandus- ja kommunikatsiooniministeeriumi
metroloogianõukogu, liige
2001-2004 TTÜ nõukogu, liige
2001-2004 TTÜ nõukogu teaduskomisjon, liige
Eesti Keevitusühing, liige
Eesti Materjalitehnika ühing, liige |
| 12. Juhendamisel kaitstud
väitekirjad | 1. Rostislav Ello, MSc, 2004, juh. Renno Veinthal.
Kiirleekpihustuspinnete väsimusomadused. Tallinn;
2. Lauri Kollo, MSc, 2003, juh. Renno Veinthal.
Tribological properties of nanocomposite TiC/DLC coatings. Tallinn |
| 13. Teadustöö põhisuunad | kulumiskindlad materjalid ja pinded, materjalide katsetamine |

Curriculum Vitae (CV)

1. First Name	Renno
2. Surname	Veinthal
3. Institution	Tallinn University of Technology, Department of Materials Engineering
4. Position	research scientist
5. Date of birth	24.07.1976
6. Education	2001-2005 doctoral study at Tallinn University of Technology, production engineering, 1999-2001 Tallinn University of Technology, production engineering, MEng; 1994-1999 Tallinn University of Technology, production engineering and transportation (five year undergraduate study) 1986-1994 Tallinn Kadrioru secondary school
7. Research and professional experience	01.09.1999 research scientist, Tallinn University of Technology 16.09.1996 engineer, Tallinn University of Technology
8. Academic degree	Master of Engineering, M.Eng
9. Dates and sites of earning the degrees	Tallinn University of Technology, 2001
10. Honours/awards	Estonian Science Academy prize for diploma work "Nondestructive testing of materials and products"
11. Research-administrative experience	2004- present Metrology Council of Ministry of Economic Affairs and Communication, member 2001-2004 TUT Council, member 2001-2004 science committee of TUT Council, member Estonian Welding Society, member Estonian Materials Engineering Society, member
12. Supervised dissertations	1. Rostislav Ello, MSc, 2004, superv. Renno Veinthal. Kiirleekpihustuspinnete väsimusomadused. Tallinn; 2. Lauri Kollo, MSc, 2003, superv. Renno Veinthal. Tribological properties of nanocomposite TiC/DLC coatings. Tallinn.
13. Current research program	wear resistant materials and coatings, materials testing

Table A1

Theoretical dimensions of the cavities at (Cr steel-VC)+WC MMC material in different hardness ranges HU1 (erodent - quartz sand 0.1...0.3 mm, $v=50$ m/s)

Mean interval hardness HU1, MPa	h_p/R		$r_n, \mu\text{m}$		F_n, N	
	$\alpha=30^\circ$	$\alpha=90^\circ$	$\alpha=30^\circ$	$\alpha=90^\circ$	$\alpha=30^\circ$	$\alpha=90^\circ$
4762	0.0137	0.0276	16.5	23.4	4.10	8.16
6140	0.0118	0.0242	15.3	21.9	4.5	9.24
7517	0.0104	0.0217	14.4	20.8	4.91	10.18
8895	0.0088	0.0196	13.3	19.7	4.92	10.89
10 273	0.0066	0.0176	11.6	18.7	4.30	11.31
11 650	0.0023	0.0155	6.8	17.6	1.68	11.28

Table A2

Theoretical dimensions of the cavities at (Cr steel-VC)+WC MMC material in different hardness ranges HV0.1 (erodent - quartz sand 0.1...0.3 mm, $v=50$ m/s)

Mean interval hardness HV0.1 MPa	h_p/R		$r_n, \mu\text{m}$		F_n, N	
	$\alpha=30^\circ$	$\alpha=90^\circ$	$\alpha=30^\circ$	$\alpha=90^\circ$	$\alpha=30^\circ$	$\alpha=90^\circ$
4540	0.0141	0.0283	16.7	23.6	3.9	7.9
7440	0.00985	0.0216	14.5	20.8	4.6	9.9
10340	0.00656	0.0176	11.4	18.7	4.2	11.3
13240	0	0.0124	0	15.7	0	10.2
16 140	0	0	0	0	0	0
19 040	0	0	0	0	0	0

Table A3

Theoretical dimensions of the cavities at (Cr steel-VC)+WC MMC material in different hardness ranges HV0.1 (erodent - quartz sand 0.1...0.3 mm, $v=50$ m/s) based on new hardness distribution

Mean interval hardness HV0.1 MPa	h_p/R		$r_n, \mu\text{m}$		F_n, N	
	$\alpha=30^\circ$	$\alpha=90^\circ$	$\alpha=30^\circ$	$\alpha=90^\circ$	$\alpha=30^\circ$	$\alpha=90^\circ$
4540	0.0141	0.0283	16.7	23.6	3.9	7.9
7440	0.00985	0.0216	14.5	20.8	4.6	9.9
9860	0.00744	0.0183	12.2	19.0	4.6	11.2
11 800	0.00068	0.0153	3.69	17.4	0.5	11.2
13 740	0	0.0112	0	14.9	0	9.6
15 690	0	0	0	0	0	0
17 630	0	0	0	0	0	0
19 570	0	0	0	0	0	0

Table A4

Theoretical dimensions of the cavities at (Cr steel-VC)+WC MMC material in different hardness ranges H_{nano} (erodent - quartz sand 0.1...0.3 mm, $v=50$ m/s)

Interval (mean) H_{nano} , MPa	h_p/R		$r_n, \mu\text{m}$		F_n, N	
	$\alpha=30^\circ$	$\alpha=90^\circ$	$\alpha=30^\circ$	$\alpha=90^\circ$	$\alpha=30^\circ$	$\alpha=90^\circ$
2100	0.0208	0.0417	20.3	28.6	2.73	5.40
3540	0.016	0.0321	17.8	25.2	3.54	7.04
4980	0.0133	0.0270	16.3	23.1	4.16	8.35
6420	0.0115	0.0236	15.1	21.6	4.63	9.44
7860	0.0097	0.0210	13.9	20.4	4.78	10.30
9300	0.0074	0.0187	12.2	19.3	4.35	10.85

Table A5

Results of calculation of erosion wear of (Cr steel-VC)+WC MMC material (erodent – quartz sand 0.1...0.3 mm, $v = 50$ m/s)

HV0.1 MPa	τ_0/e_s	p_i		I_g^P , mg/kg Eq. (1.1)		I_g^B , mg/kg Eq. (1.2)		I_g , mg/kg	
		30°	90°	30°	90°	30°	90°	30°	90°
4762	0.15	0	0	54.0	56.6	0	0	11.5	12.1
6140		0	0	39.1	43.4	0	0	9.58	10.6
7517	0.5	0.995	0.423	298	346	2825	4079	271	804
8895		1	0.425	227	282	2598	3876	137	429
10 273		1	0.308	161	228	2261	3674	33.2	151
11 650		1	0.019	70	176	1327	3444	0.9	33.2
								463	1440

Table A6

Results of calculation of erosion wear of (Cr steel-VC)+WC MMC material (erodent – quartz sand 0.1...0.3 mm, $v = 50$ m/s)

HV0.1 MPa	τ_0/e_s	p_i		I_g^P , mg/kg Eq. (1.1)		I_g^B , mg/kg Eq. (1.2)		I_g , mg/kg	
		30°	90°	30°	90°	30°	90°	30°	90°
4540	0.1	0	0	52.8	54.9	0	0	39.3	40.9
7440		0	0	26.7	31.9	0	0	0.9	1.1
10 340	0.5	0.54	1.0	1290	3664	2239	3664	6.9	75.8
13 240		0	1.0	0	3081	0	3081	0	185
16 140		0	0	0	0	0	0	0	0
19 040		0	0	0	0	0	0	0	0
								49.6	176.0

Table A7

Results of calculation of erosion wear of (Cr steel-VC)+WC MMC material (erodent – quartz sand 0.1...0.3 mm, $v = 50$ m/s) based on new hardness distribution

HV0.1 MPa	τ_0/e_s	p_i		I_g^P , mg/kg Eq. (1.1)		I_g^B , mg/kg Eq. (1.2)		I_g , mg/kg	
		30°	90°	30°	90°	30°	90°	30°	90°
4540	0.1	0	0	52.8	54.9	0	0	39.3	40.9
7440		0	0	26.7	31.9	0	0	0.9	1.1
9860	0.5	0.627	1	1563	3736	2383	3736	5.9	13.3
11 800		0.0014	1	367	3416	721	3416	0.4	39.4
13 740		0	1	0	2921	0	2921	0	85.4
15 690		0	0	0	0	0	0	0	0
17 630		0	0	0	0	0	0	0	0
19 570	0	0	0	0	0	0	0	0	
								46.2	180.0

Table A8

Results of calculation of erosion wear of (Cr steel-VC)+WC MMC material (erodent – quartz sand 0.1...0.3 mm, $v = 50$ m/s)

H_{nano} MPa	τ_0/e_s	p_i		I_g^P , mg/kg Eq. (1.1)		I_g^B , mg/kg Eq. (1.2)		I_g , mg/kg	
		30°	90°	30°	90°	30°	90°	30°	90°
2100	0.05	0	0	66.6	59.6	0	0	20.4	18.3
3540				35.7	35.3			11.6	11.4
4980				23.6	24.9			4.88	5.17
6420	0.5	0.039	0.289	132.0	148.0	360.7	517.1	14.6	26.3
7860		0.043	0.358	97.8	117.0	331.4	487.8	4.67	10.8
9300		0.033	0.404	68.6	92.6	290.2	459.9	1.19	3.78
								57.3	75.8

Table A9

Theoretical dimensions of the cavities at NiCrSiB + (WC-Co) MMC coating in different hardness ranges (erodent – quartz sand 0.1...0.3 mm, $v=50$ m/s)

Interval (mean) HU1, MPa	h_p/R		r_n , μm		F_n , N	
	$\alpha=30^\circ$	$\alpha=90^\circ$	$\alpha=30^\circ$	$\alpha=90^\circ$	$\alpha=30^\circ$	$\alpha=90^\circ$
1177	0.045	0.089	29.5	41.3	3.228	6.309
2392	0.031	0.062	24.8	34.8	4.633	9.120
3606	0.025	0.051	22.4	31.5	5.697	11.26
4820	0.022	0.044	20.8	29.4	6.565	13.05
6034	0.020	0.039	19.7	27.8	7.351	14.63
7248	0.018	0.036	18.7	26.5	7.798	16.02

Table A10

Theoretical dimensions of cavities at NiCrSiB + (WC-Co) MMC coating in different hardness ranges (erodent- granite gravels 2.8... 5.6 mm at velocity 80 m/s and in different hardness ranges)

Interval (mean) HU1, MPa	h_p/R		r_n , mm		F_n , N	
	$\alpha=30^\circ$	$\alpha=90^\circ$	$\alpha=30^\circ$	$\alpha=90^\circ$	$\alpha=30^\circ$	$\alpha=90^\circ$
1177	0.045	0.089	0.739	1.03	2018	3943
2392	0.031	0.062	0.621	0.871	2892	5699
3606	0.025	0.051	0.561	0.788	3561	7038
4820	0.022	0.044	0.521	0.734	4103	8155
6034	0.020	0.039	0.492	0.695	4594	9146
7248	0.018	0.036	0.468	0.663	4986	10 015

Table A11

Results of calculation of erosion wear of NiCrSiB + (WC-Co) MMC coating (erodent – quartz sand 0.1...0.3 mm, $v = 80$ m/s)

HU1 MPa	τ_0/e_s	p_i		I_g^P , mg/kg Eq. (1.1)		I_g^B , mg/kg Eq. (1.2)		I_g , mg/kg	
		30°	90°	30°	90°	30°	90°	30°	90°
1177	0.06	0	0	597	393	0	0	176	116
2392				254	193			72	55
3606				155	128			29	24
4820				109	96			11	10
6034	0.15	0.616	0.944	339	311	799	1132	29	50
7248		0.664	0.964	270	258	759	1080	11	19
								328	274

Table A12

Results of calculation of erosion wear of NiCrSiB + (WC-Co) MMC coating (erodent – granite gravels 2.8...5.6 mm, $v = 80$ m/s)

HU1 MPa	τ_0/e_s	p_i		I_g^P , mg/kg Eq. (1.1)		I_g^B , mg/kg Eq. (1.2)		I_g , mg/kg	
		30°	90°	30°	90°	30°	90°	30°	90°
		1177	0	0.002	597	393	550	777	145
2392	0.06	0.001	0.004	254	193	460	651	59	45.3
3606		0.002	0.006	155	128	415	587	24.2	20.3
4820		0.002	0.007	109	96	385	546	9.19	8.28
6034		0.15	1	1	339	311	6827	9682	260
7248	1		1	270	258	6487	9236	97.2	138
								722	821

Kulu, P., Veinthal, R.
Selection criteria for abrasive erosion wear resistant powder coatings.
Materials Science (Medžiagotyra), Vol. 8, No 4, 2002, pp. 409–412.

Veinthal, R., Kulu, P., Käerdi, H.
Characterization of the structure of composite powder materials and coatings.
Materials Science (Medžiagotyra), Vol. 11, No. 4, 2005, pp. 376–380.

Paper III

Kulu, P., Veinthal, R., Käerdi, H.
Modelling of erosion wear of powder composite materials and coatings.
International Journal of Tribology (submitted)

Paper IV

Kulu, P., Hussainova, I. and Veinthal, R.
Solid particle erosion of thermal sprayed coatings.
Wear, Vol. 258, 1–4, 2005, p. 488–496.

Paper V

Kulu, P., Veinthal, R.

Wear resistance of high velocity thermal sprayed coatings.
Proc. of 9th Nordic Symposium on Tribology NORDTRIB 2000,
VTT of Finland, Espoo, Finland, 2000, Vol. 1, pp. 87–95.

Paper VI

Kulu, P., Veinthal, R., Kõo, J., Lille, H.
Mechanism of abrasion erosion wear of thermal sprayed coatings.
*Proc. of the Conference EUROMAT 2000 on Advances in Mechanical Behaviour,
Plasticity and Damage*, Tours, France, 2000, pp. 651–656.